Simulations of relativistic plasma dynamics and jet acceleration in PWNe and GRB progenitors

Luca Del Zanna

Dipartimento di Astronomia e Scienza dello Spazio
Università di Firenze

Dipartimento di Fisica e Astronomia
Università di Firenze

In collaboration with: N. Bucciantini, O. Zanotti, E. Amato, D. Volpi, P. Londrillo

Part I: Pulsar Wind Nebulae

- Why are Pulsar Wind Nebulae so important?
  - Composition, magnetization and anisotropy of pulsar wind
  - Acceleration of particles at relativistic shocks
  - Standard candles for other synchrotron and IC sources
  - Dynamics of relativistic plasmas
  - Jet-torus structure, acceleration or relativistic jets
- They are a unique laboratory to investigate relativistic outflows and their interaction with the environment
  - GRBs
  - AGN jets

Probing Pulsar Winds: PWNe

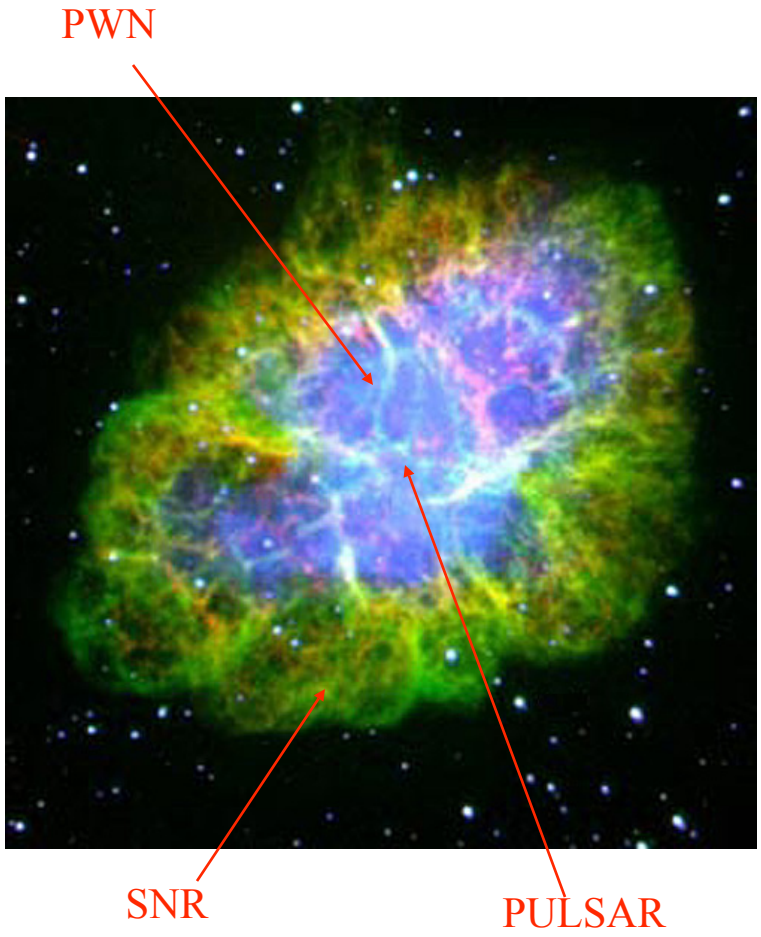

- PWNe are hot bubbles (also called plerions) of relativistic particles and magnetized plasma emitting non-thermal radiation (synchrotron - IC) from radio to γ
- Originated by the interaction of the ultra-relativistic magnetized pulsar wind with the expanding SNR (or with the ISM)
- Crab Nebula in optical: central amorphous mass (continuum) and external filaments (lines)

Sketch of PWN / SNR interaction

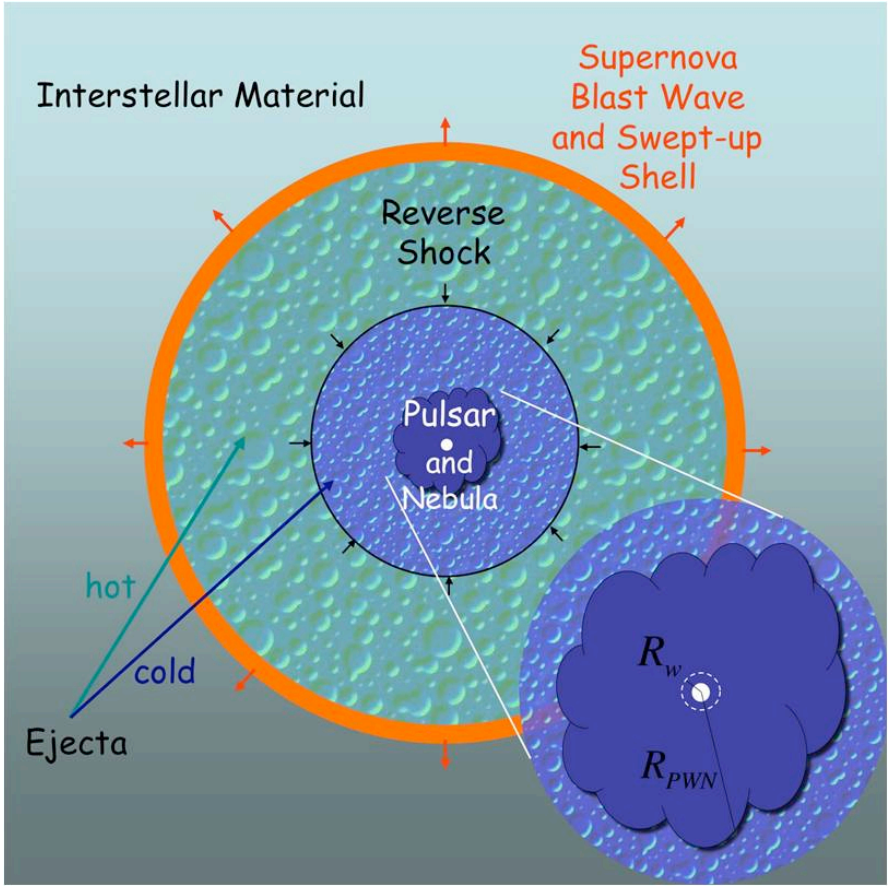

(Gaensler & Slane, 2006)

- The SNR consists of dense ejecta: formation of a blast wave expanding in the ISM and a reverse shock
- The ultrarelativistic pulsar wind inflates a plerion inside the SNR, not affecting the overall evolution

$$E_{snr} = 10^{51}\ \text{erg}$$
$$E_{pw} = 10^{49}\ \text{erg}$$

PWN-SNR: 1-D structure and evolution

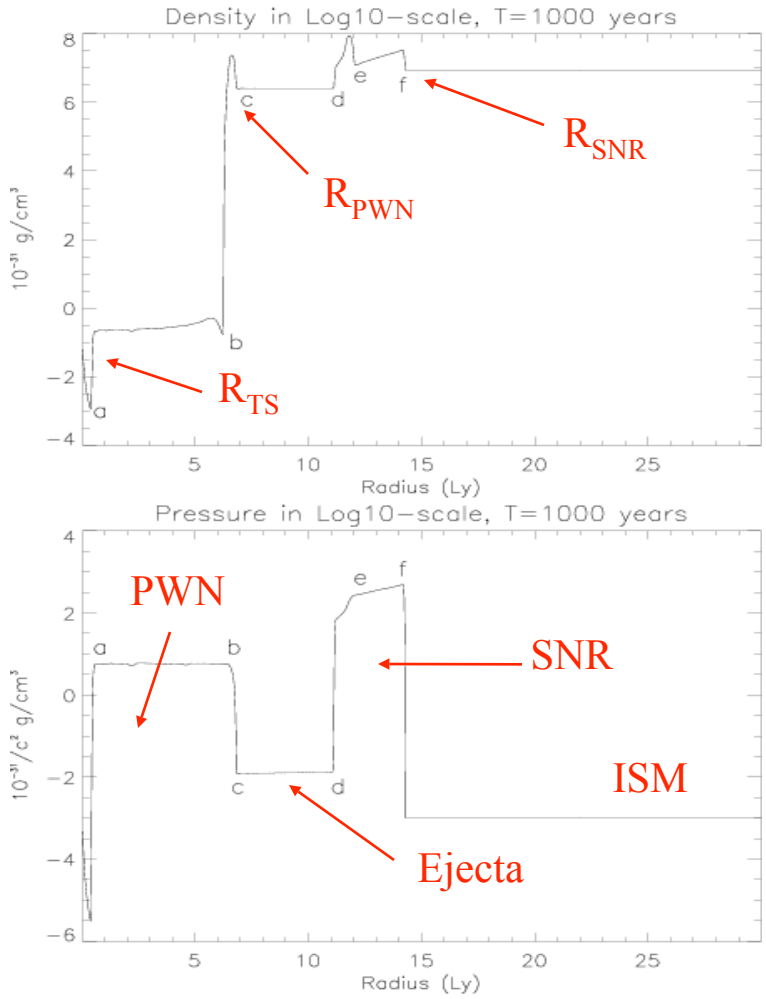

- a: pulsar wind termination shock
- b: PWN-SNR contact discontinuity
- c: swept-up ejecta ($R_{PWN} \propto t^{6/5}$)
- d: SNR reverse shock
- e: SNR contact discontinuity
- f: SNR forward shock

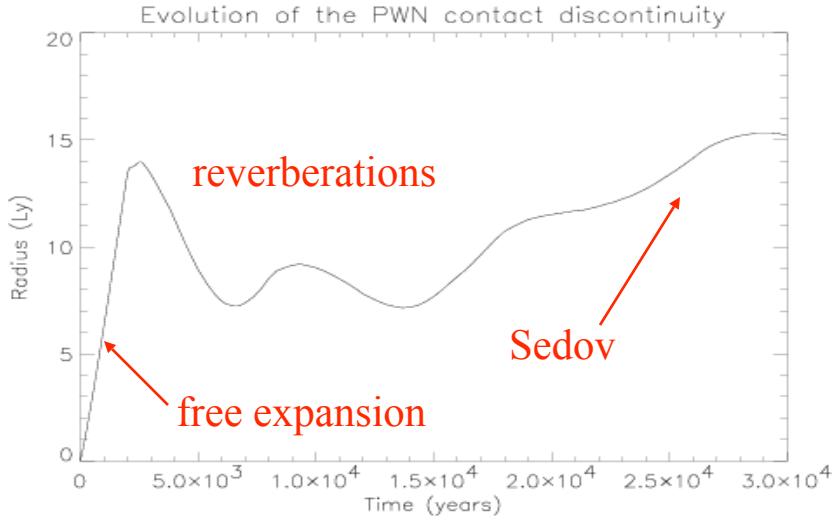

Jet-torus structure: Chandra X-ray images

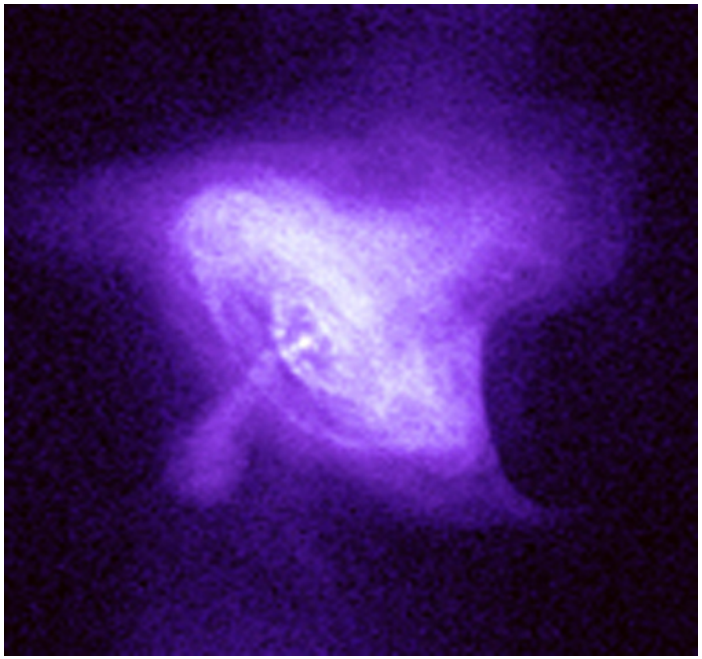

Crab

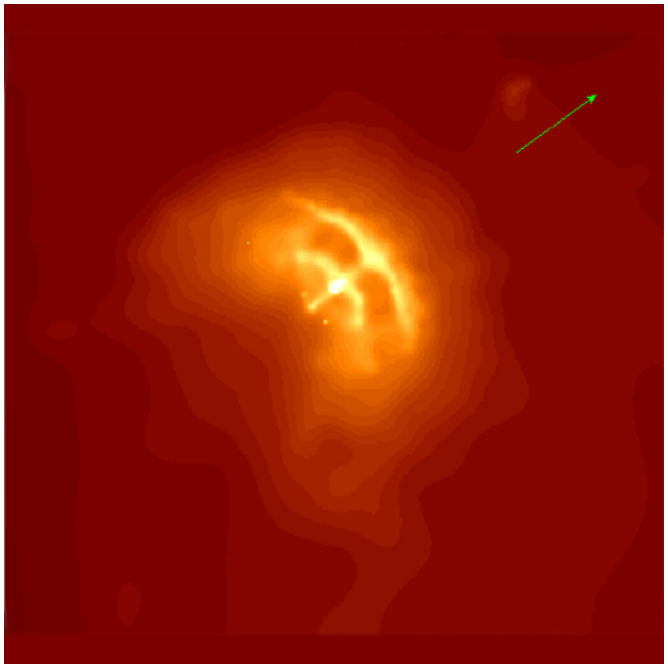

Vela

- Equatorial torus of enhanced emission, rings and jets!
- We need to move from spherical to axisymmetric models

How common is the jet-torus structure?

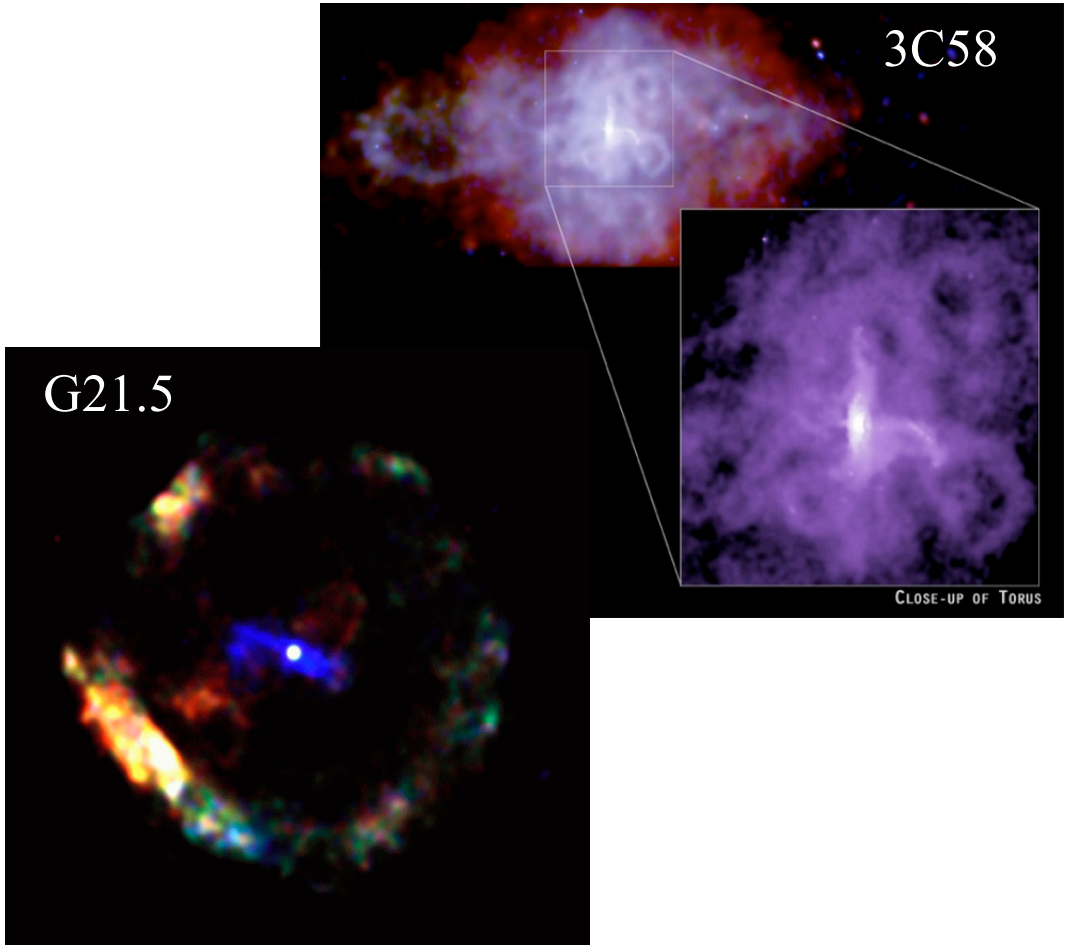

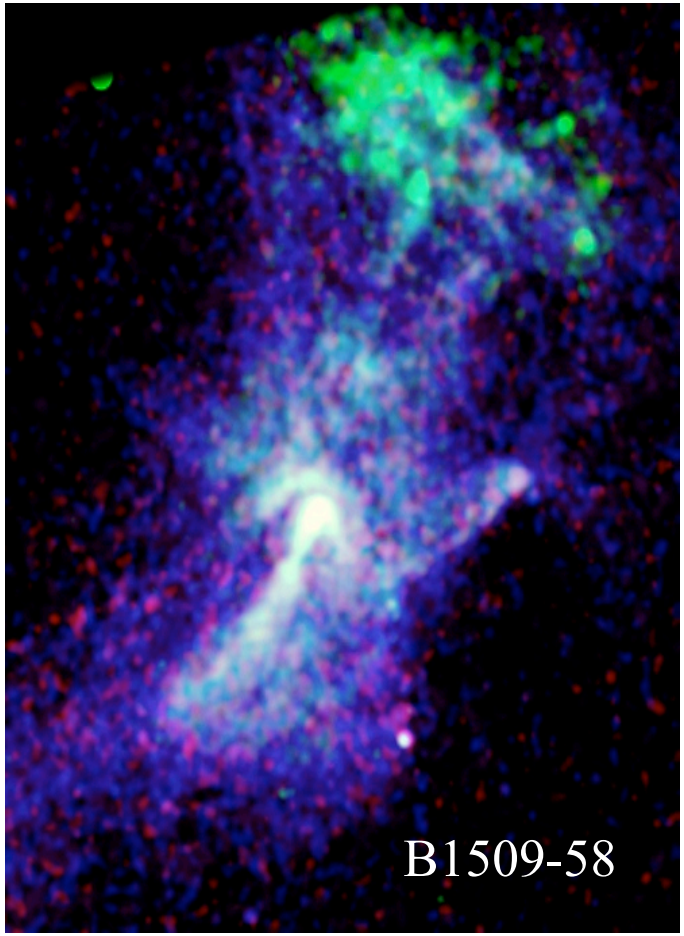

Relativistic motions and time variability

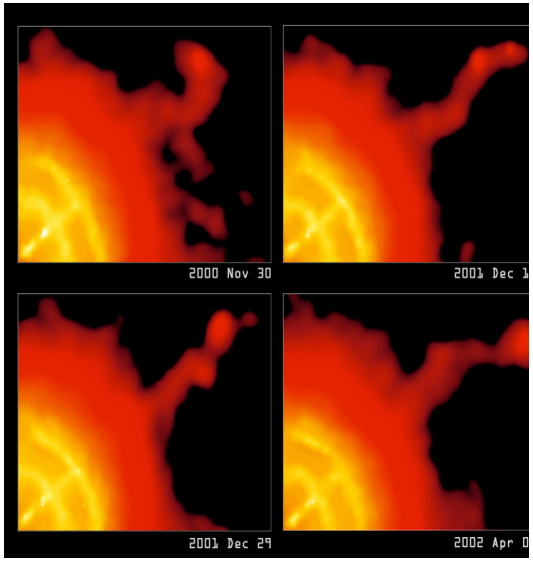

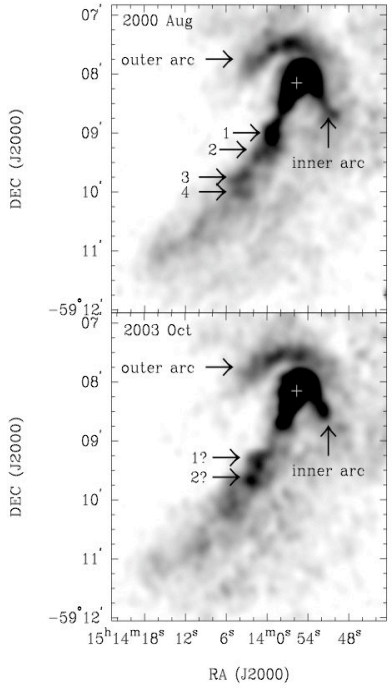

Crab

Vela

B1509-58

- Equatorial motions (wisps): v=0.3-0.5 c
  - Timescale of months-year: MHD or gyrating ions?
- Polar jet motions: v=0.5-0.8 c

Relativistic motions and time variability

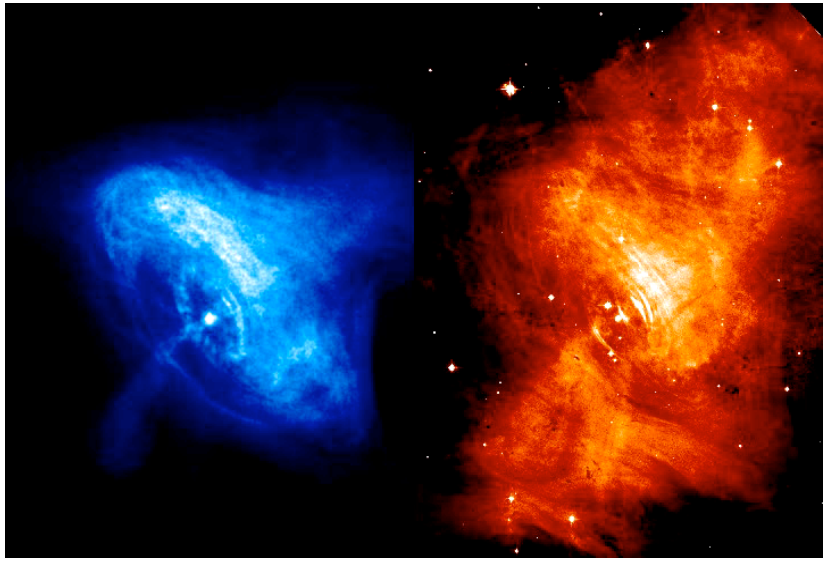

Crab

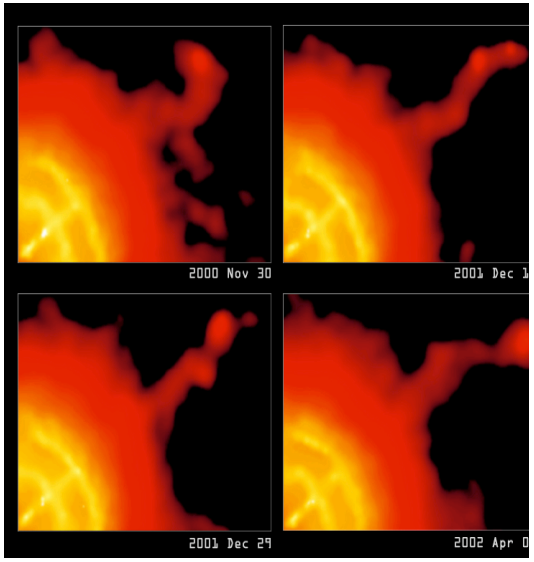

Vela

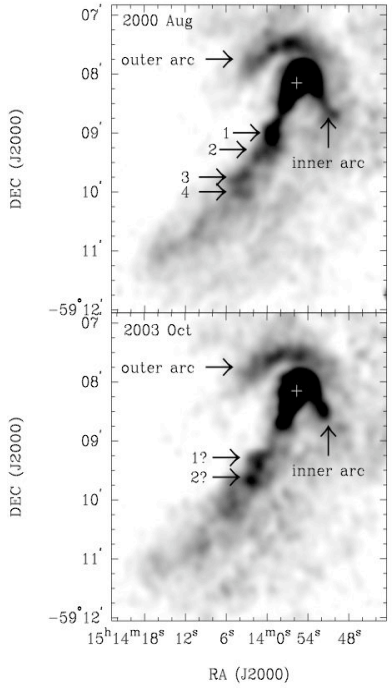

B1509-58

- Equatorial motions (wisps): v=0.3-0.5 c
  - Timescale of months-year: MHD or gyrating ions?
- Polar jet motions: v=0.5-0.8 c

Jet-torus structure: theory

- Torus: higher equatorial energy flux
- Jets: magnetic collimation. But in PW:

$$\gamma >> 1 \Rightarrow \rho_q \vec{E} + \vec{j} \times \vec{B} \approx 0$$

collimation downstream of the TS?

  - *Lyubarsky, 2002*
  - *Bogovalov & Khangoulian, 2002, 2003*

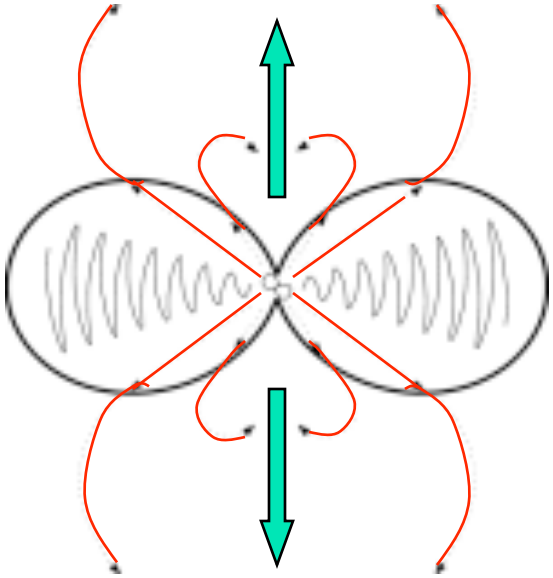

- Axisymmetric RMHD simulations of the interaction of an anisotropic relativistic magnetized wind with SN ejecta
  - *Komissarov & Lyubarsky, 2003, 2004*
  - *Del Zanna, Amato & Bucciantini, 2004*

Axisymmetric relativistic wind model

- Far from the pulsar light cylinder the wind is expected to be ultrarelativistic, cold, and weakly magnetized. We assume:
  - Isotropic mass flux, anisotropic energy flux $(F \propto r^2 \rho \gamma^2 \propto \gamma)$:

$$\gamma(\theta) = \gamma_0[\alpha + (1-\alpha)\sin^2(\theta)]$$

  - Purely toroidal magnetic field (split monopole):

$$B(r,\theta) = B_0(r_0/r)\sin(\theta)$$

  - Parameters of the wind model:

$$\gamma_o >> 1,\ \alpha = \frac{F(0)}{F(\pi/2)} << 1,\ \sigma = \frac{B_0^2}{4\pi c^2 \rho_0 \gamma_0^2} << 1$$

TS structure and flow pattern

- The wind anisotropy shapes the TS structure. A complex flow pattern arises:
  - A: ultrarelativistic pulsar wind
  - B: subsonic equatorial outflow
  - C: supersonic equatorial funnel
  - D: super-fastmagnetosonic flow
  - a: termination shock front
  - b: rim shock
  - c: fastmagnetosonic surface

σ=0.003

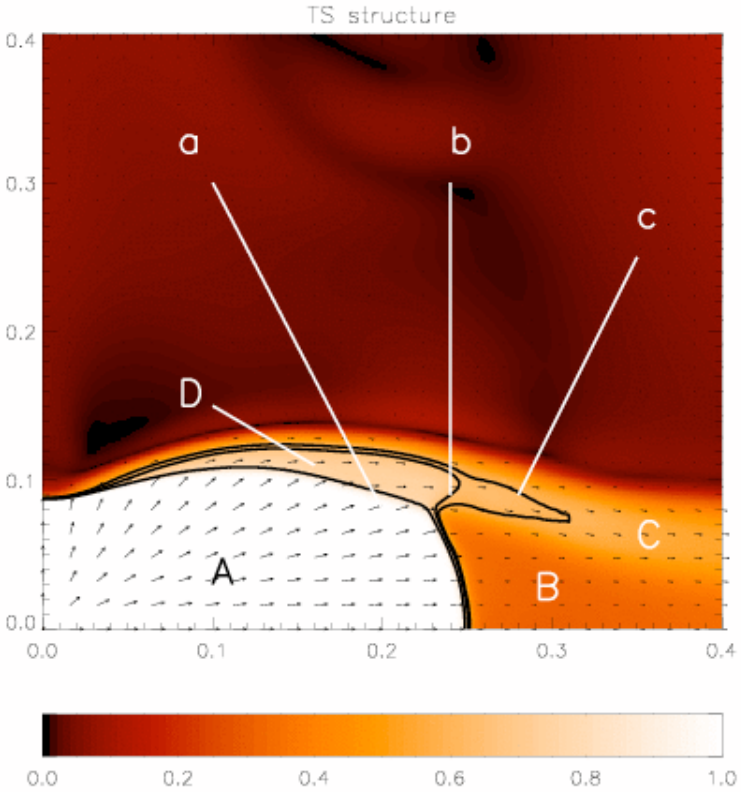

Formation of polar jets by hoop stresses

- The flow pattern changes drastically with increasing σ
- For high magnetization (σ>0.01) a supersonic jet is formed

σ=0.003

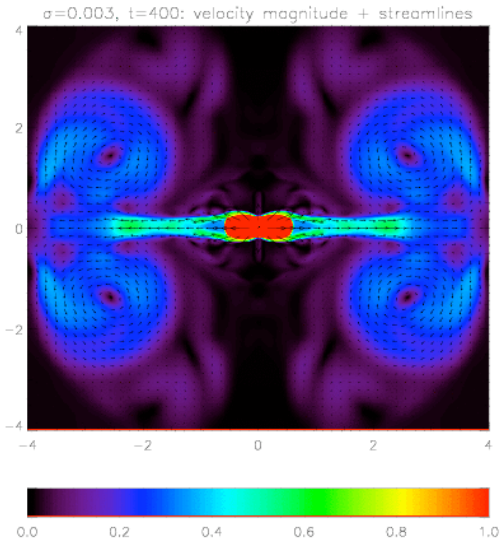

σ=0.01

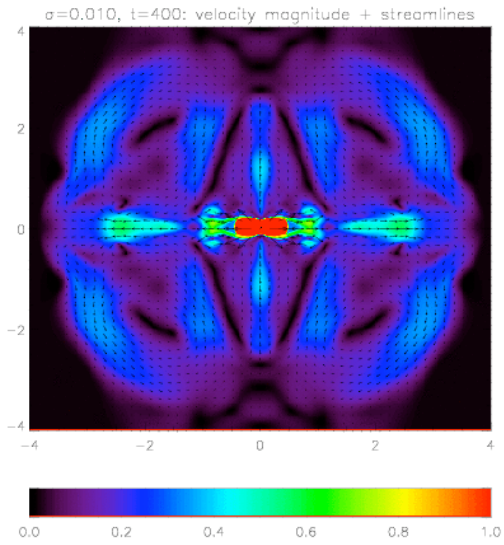

σ=0.03

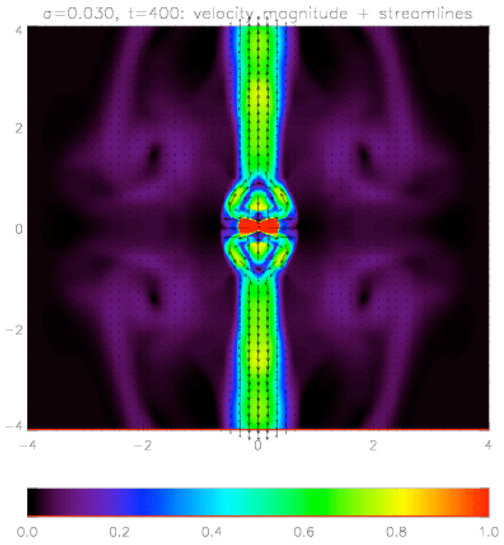

Dependence on the field shape

- Wind magnetic field with an equatorial neutral sheet

$$B(r,\theta) = B_0 \left(\frac{r_0}{r} \right) \sin(\theta)\ \tanh[b(\pi/2 - \theta)]$$

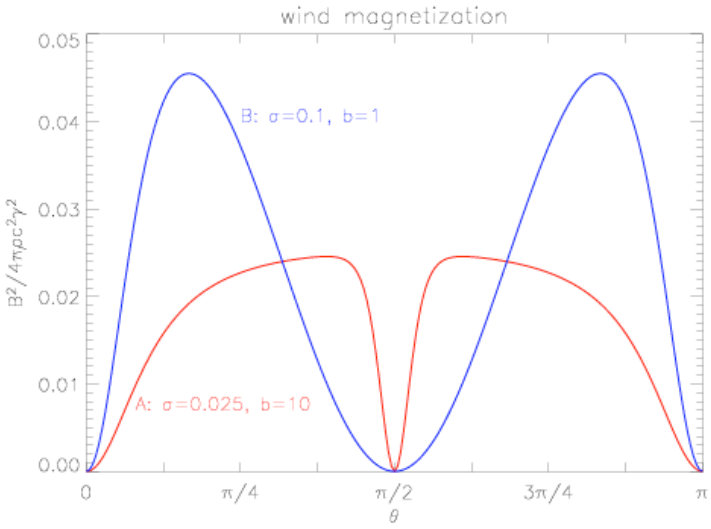

Two runs with effective σ=0.02:
(A: σ=0.025, b=10, B: σ=0.1, b=1)

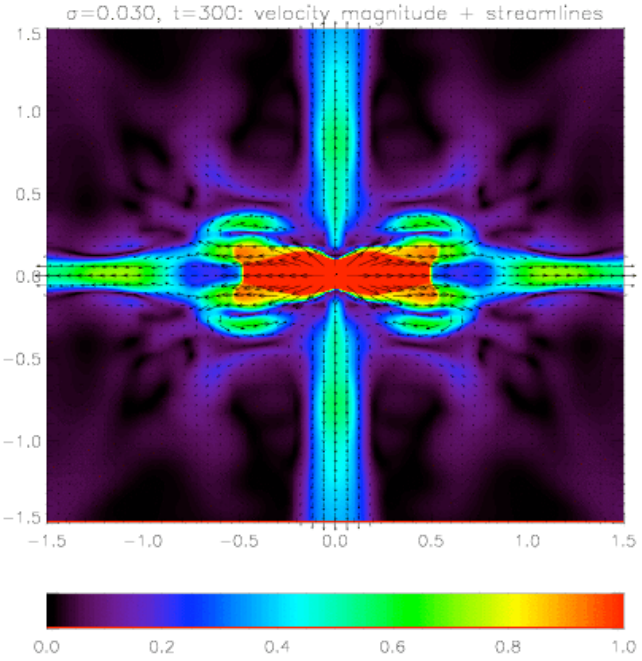

Synchrotron diagnostic for RMHD codes

- Simple recipes to work out synchrotron emission:
  - Assume a power law spectrum at the accelerating sites (here TS)
  - Write local particles distribution as a function of a cut-off energy
  - Evolve the cut-off energy including adiabatic and synchrotron losses
  - Calculate emissivity in the comoving frame at a given frequency
  - Calculate Lorentz transformations to the observer's frame
  - Integrate along line of sight
- A complete suite of diagnostic tools for RMHD simulations:
  - Surface brightness maps
  - Polarization maps
  - Spectral index maps, integrated spectra
- Reference: *Del Zanna, Volpi, Amato, Bucciantini, 2006, A&A 453, 621*

Flow dynamics and energy losses

- Particles are injected at TS with $\varepsilon_\infty = E/m_e c^2 = 10^9$
- Stronger synchrotron losses occur along TS and in the torus, where magnetization is higher
- The flow pattern allows emission also in polar jets

velocity

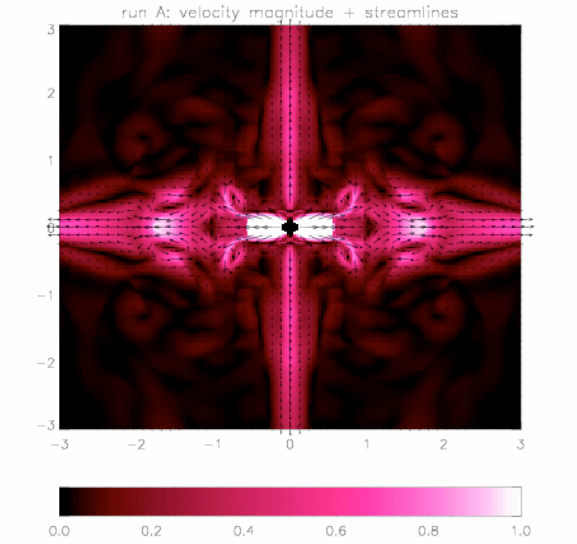

magnetization

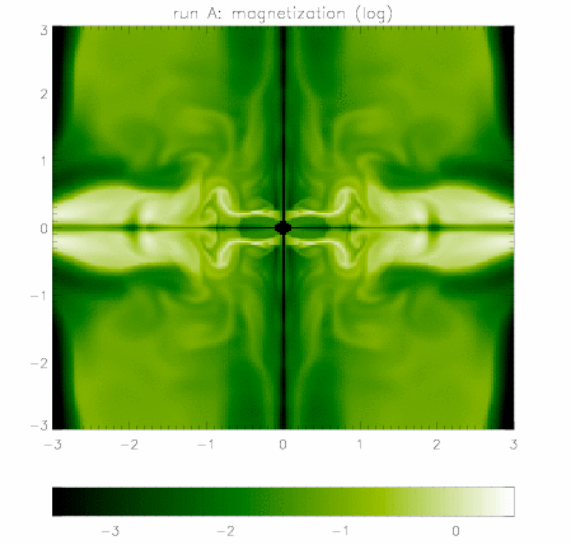

max energy

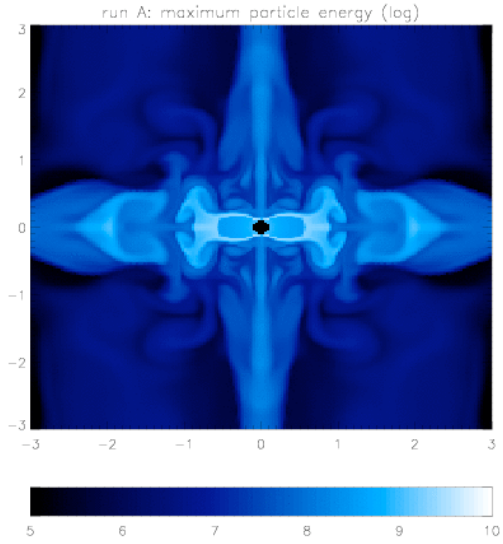

Comparison with observations

- Simulated X-ray maps vs Chandra images:

Run A: σ=0.025, b=10

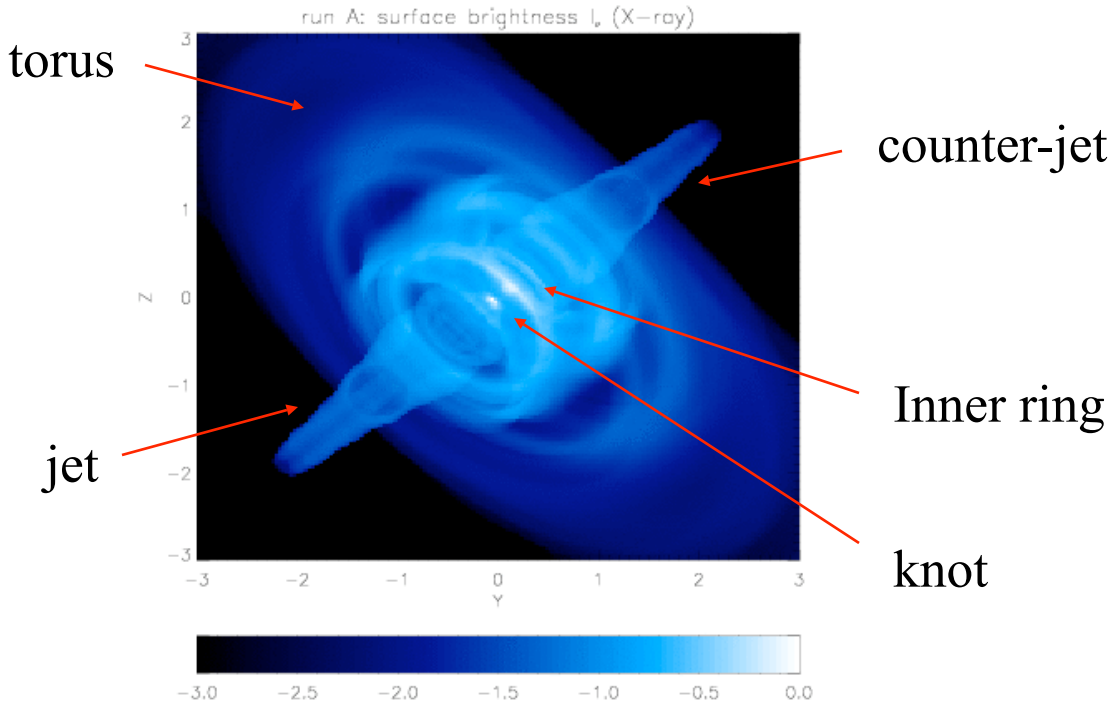

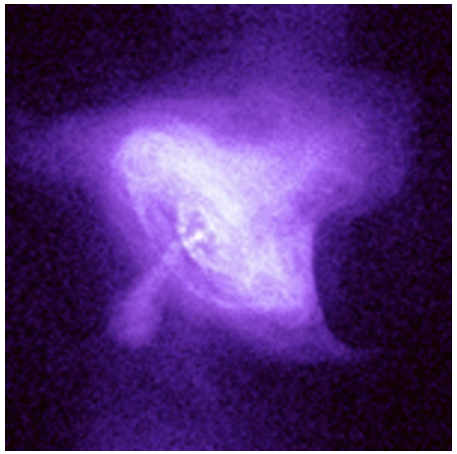

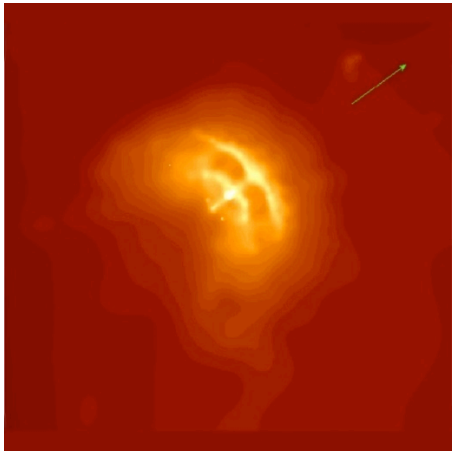

Doppler boosted features

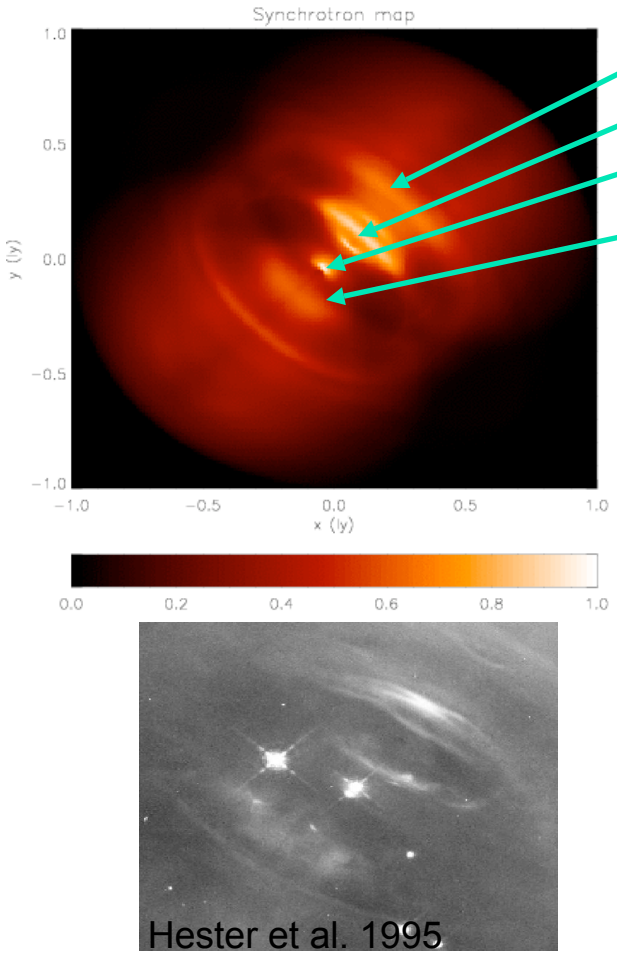

Main torus
Inner ring (wisps structure)
Knot
Back side of the inner ring

No jet - Axisymmetric assumption

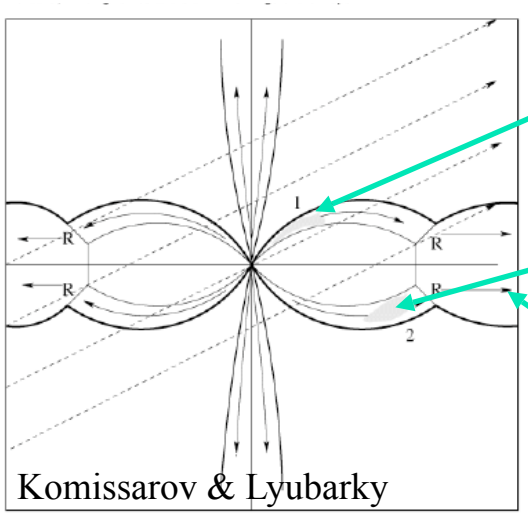

Knot

Ring

Torus

Towards the best match with CN

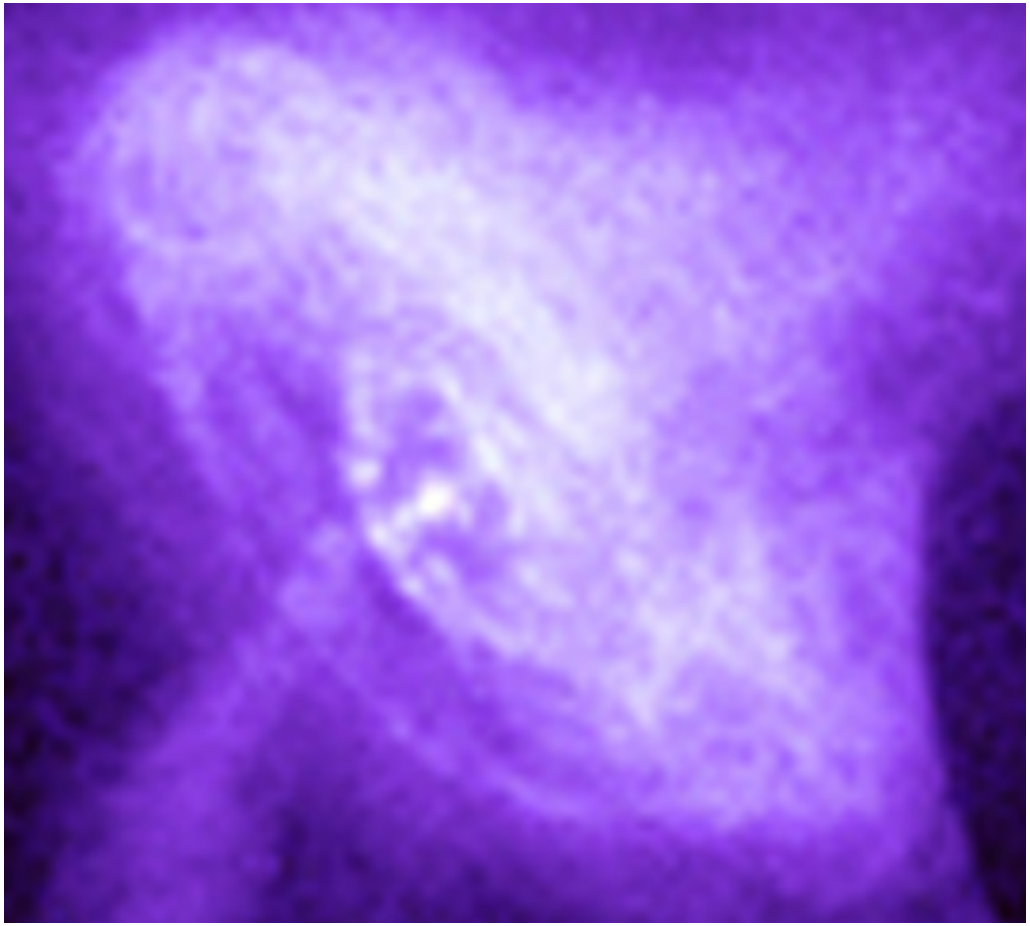

(Camus et al., 2009)

Towards the best match with CN

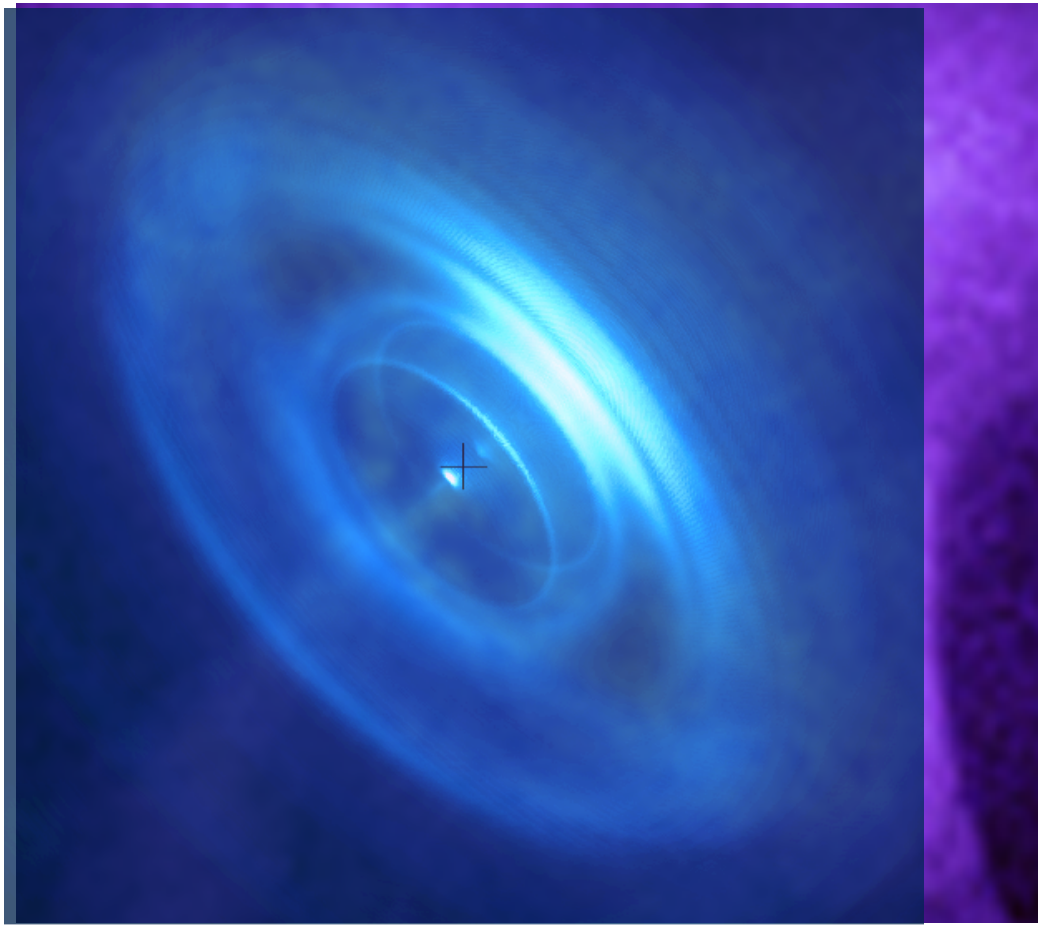

(Camus et al., 2009)

Additional diagnostics: spectral index maps

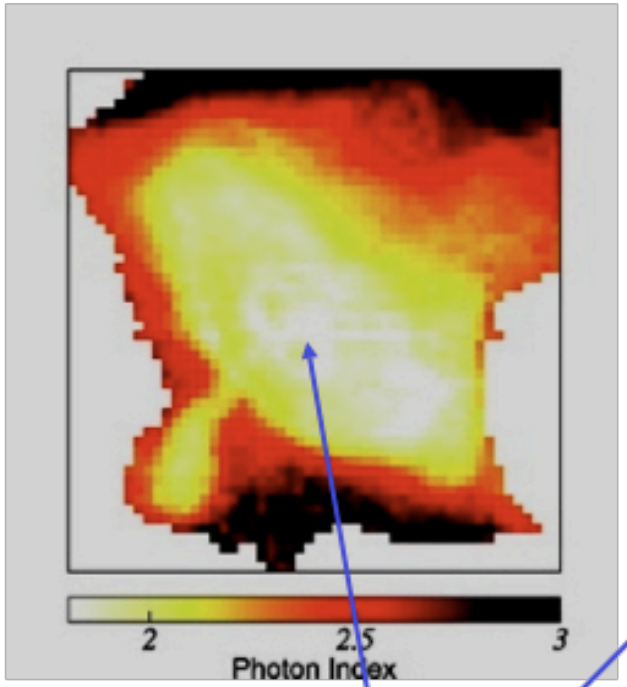

Mori

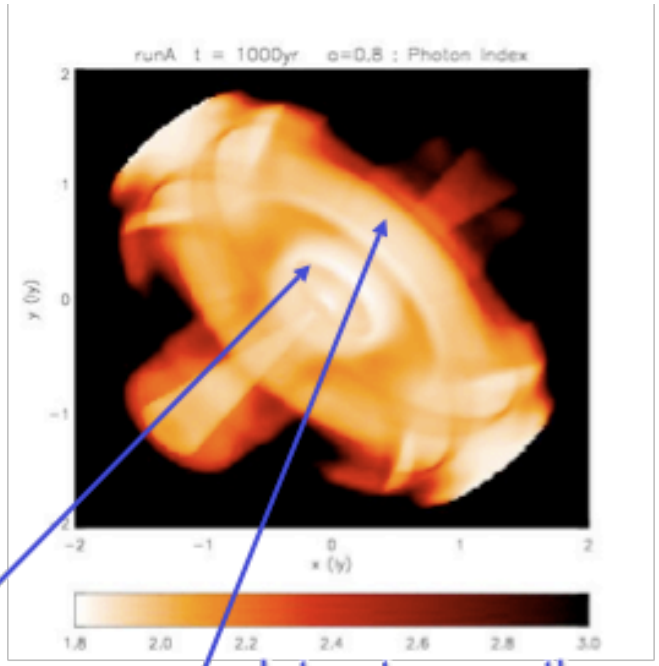

Jet not correctly reproduced

(required reacceleration)

Higher index in the torus

(recompression and boosting)

Brighter inner ring

Additional diagnostics: polarization maps

- A powerful diagnostic tool for B and v in PWNe, however high-resolution optical (and X-ray!) maps are still missing

Polarization fraction

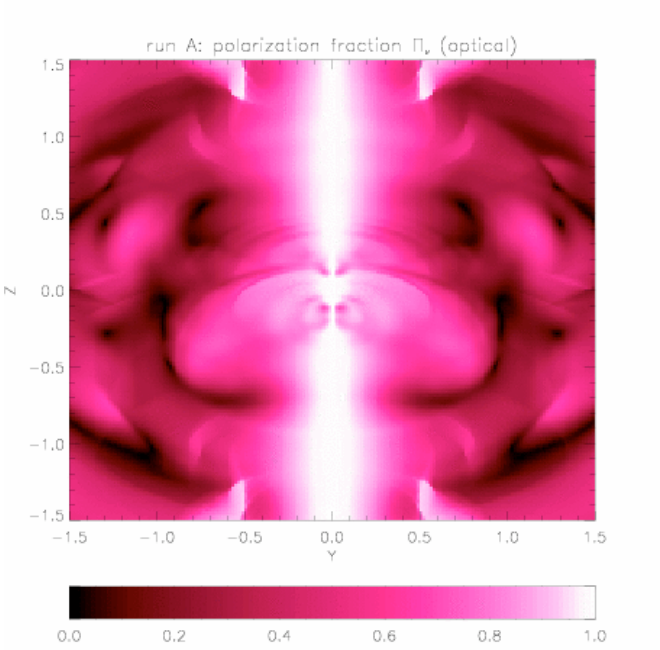

Run A

Polarization direction

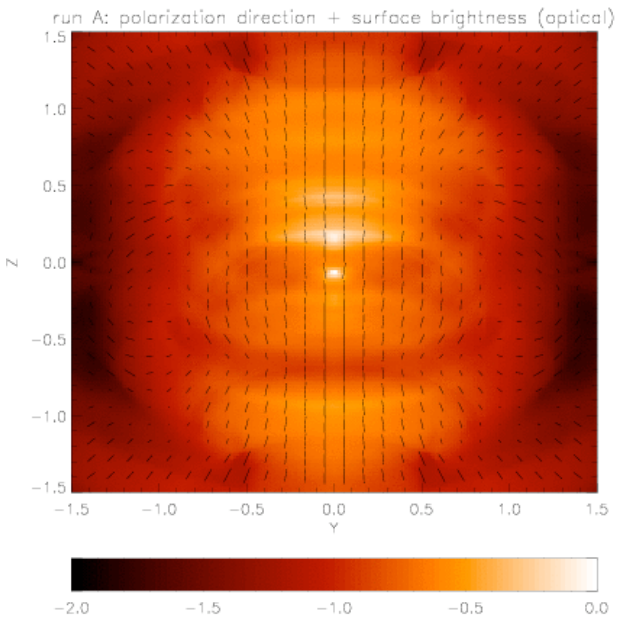

Optical polarization summary

Toroidal field in the inner portion of the nebula and the torus

Polarization in the wisps ~ 25-35%
Peak polarization ~ 40%
Knot polarization ~ 50%
Variability !!

Polarization angle in wisps and knot is aligned with PSR and nebular axis

Toroidal field

Poloidal-like field structure might be due to angle swing

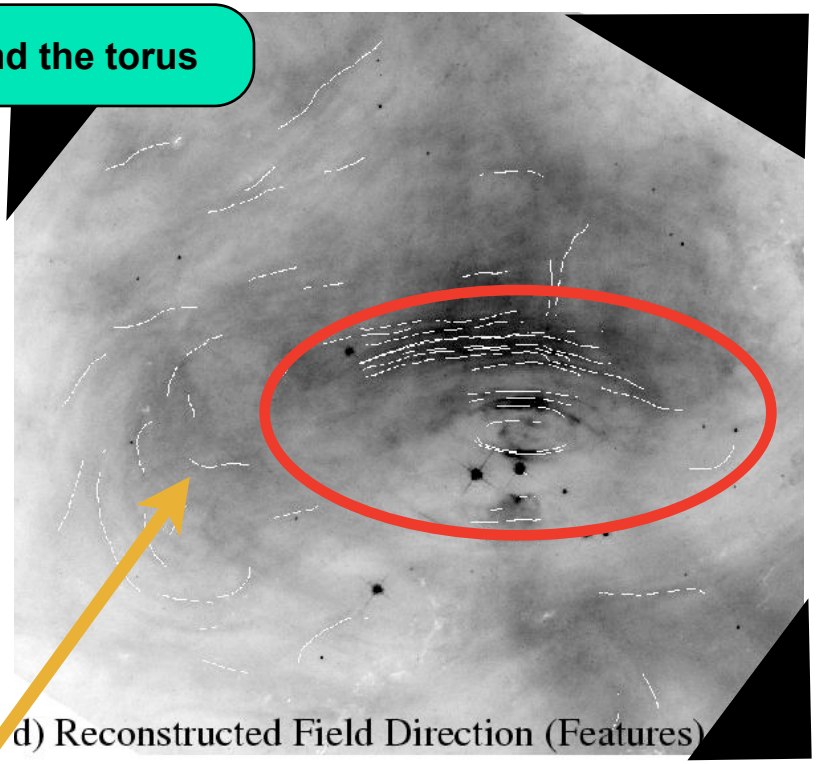

Hester 08

Relativistic angle swing

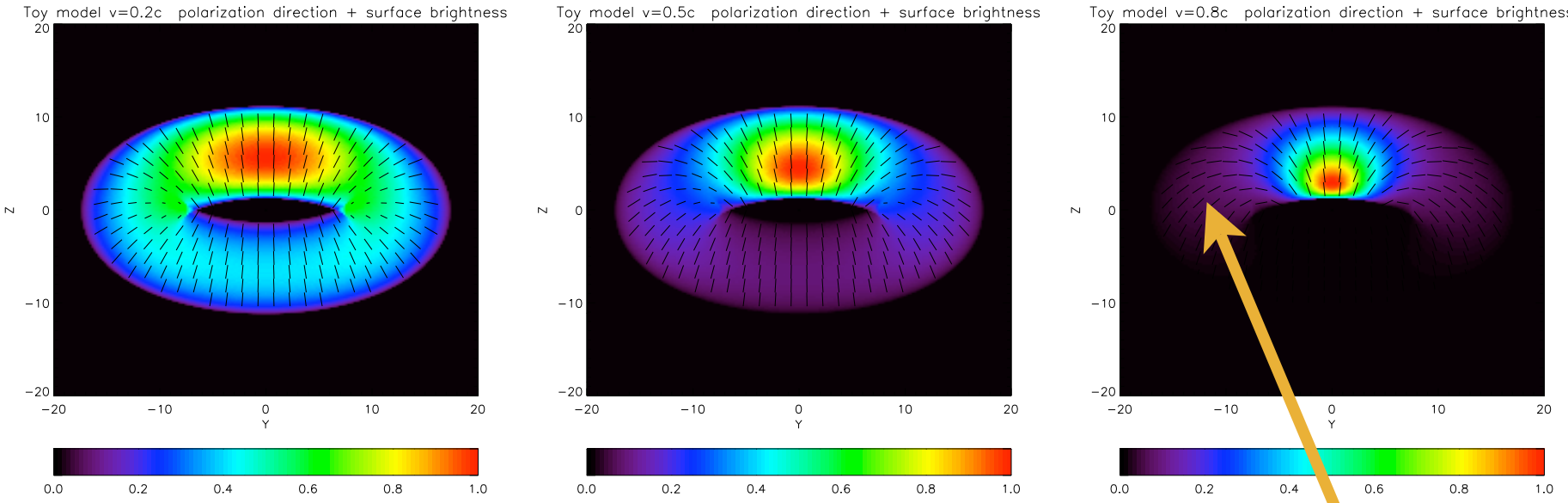

Bucciantini et al. 05

Inferred direction of the magnetic field is affected by relativistic boosting and Lorentz transformation

Toroidal field looks like poloidal at the edges

γ-rays from Pulsar Wind Nebulae

- Particles are accelerated at TS up to energies >10^{15} eV (the pulsar voltage!)
- MeV-GeV gamma-rays produced by the high energy tail as synchrotron
- GeV-TeV gamma-rays produced by IC scattering and/or hadronic contributions
- PWNe are the best estabilished galactic TeV sources
- TeV PWNe are being identified by HESS, MAGIC…

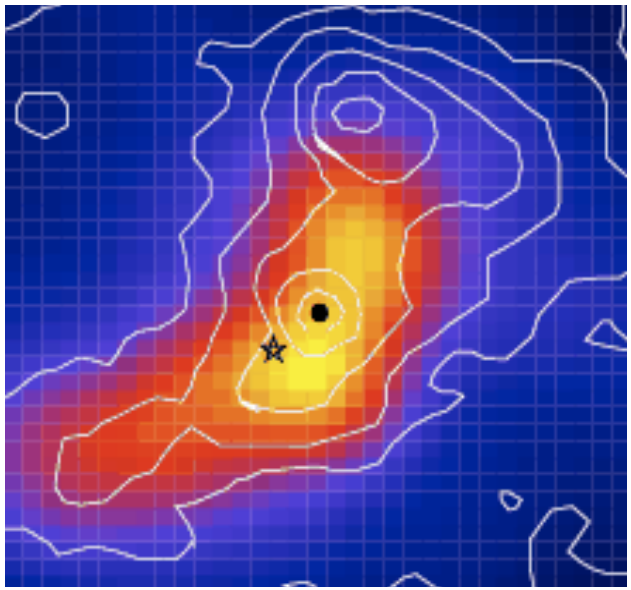

B1509-58 (HESS; Aharonian et al. 2005)

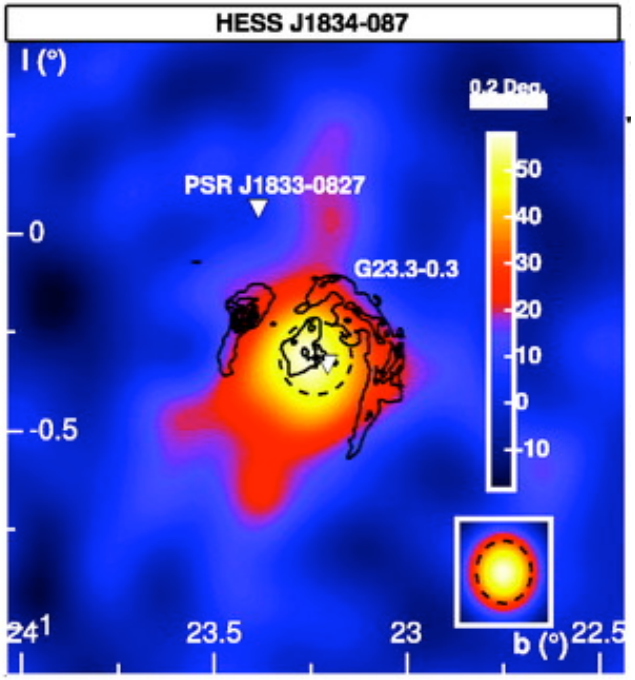

J1834-087 (HESS; Aharonian et al. 2005)

A poweful diagnostic tool: IC scattering

- Leptonic model: both the optical / X-ray / MeV synchrotron and the higher energy gamma spectral components are due to the same ultra-relativistic electrons accelerated at TS
- GeV-TeV emission due to Inverse Compton scattering off a photon background (synchrotron, starlight, FIR, CMB)
- Combined X-ray and γ-ray observations may help to disentangle the electron density and the magnetic field:

$$L_X \propto n_e B^2, L_{IC} \propto n_e n_{ph}; \quad L_X / L_{IC} \Rightarrow B$$

- For a uniform photon field, IC emission provides direct information about the relativistic electron distribution
- IC diagnostics added (*Volpi, Del Zanna, Amato, Bucciantini, 2008*)

IC emission recipes

- Two particle populations (*Atoyan & Aharonian 1996*):
  - wind electrons: accelerated at TS and suffering adiabatic and radiative losses, density and local maximum energy evolved by the code

$$f_0(\varepsilon_0) = \frac{A_O}{4\pi}(\bar{\varepsilon}_0 + \varepsilon_0)^{-(2a_w+1)} \exp(-\varepsilon_0/\varepsilon_0^c) \Rightarrow f_w(\varepsilon) = (\rho/\rho_0)^{4/3}(\varepsilon_0/\varepsilon)^2 f_0(\varepsilon_0); \quad \varepsilon_0 = (\rho_0/\rho)^{1/3}\frac{\varepsilon}{1-\varepsilon/\varepsilon_\infty}$$

  - relic radio electrons: steady and homogeneous population

$$f_R(\varepsilon) = \frac{A_R}{4\pi}\varepsilon^{-(2\alpha_R+1)}\exp(-\varepsilon/\varepsilon_R^C)$$

  - IC spectral emissivity (complete Klein-Nishina cross section):

$$j_\nu^{IC}(\nu) = \int P_\nu^{IC}(\nu,\varepsilon) f(\varepsilon) d\varepsilon; \quad P_\nu^{IC}(\nu,\varepsilon) = ch\nu \int \frac{d\sigma}{d\nu_t}(\nu_t,\nu,\varepsilon) n_t(\nu_t) d\nu_t$$

  - Photon densities:

$$n_\nu^{IC-SYN}(r,\nu_t) = \frac{1}{ch\nu_t}\frac{L_\nu^{FIR}(\nu_t)}{4\pi R^2}U(r/R); \quad n_\nu^{IC-CMB}(\nu_t) = \frac{8\pi}{c^3}\frac{\nu_t^2}{\exp(h\nu_t/k_BT)-1}$$

First γ-ray surface brightness maps

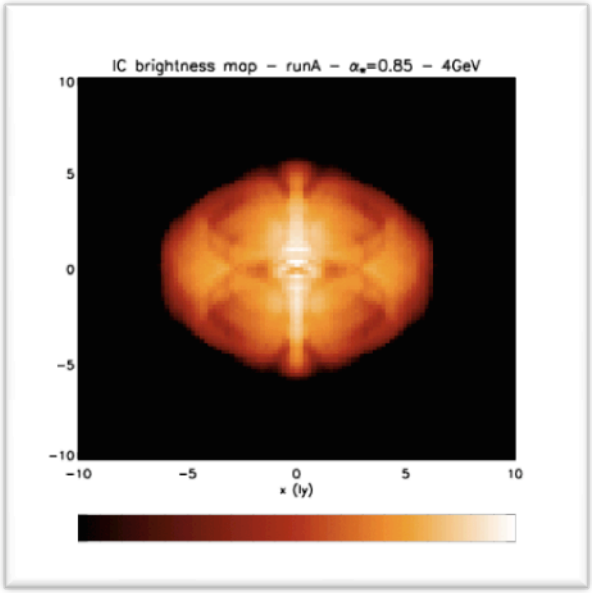

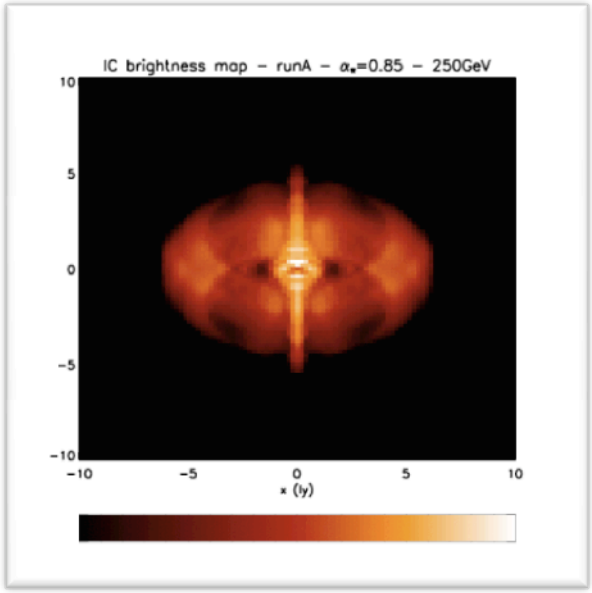

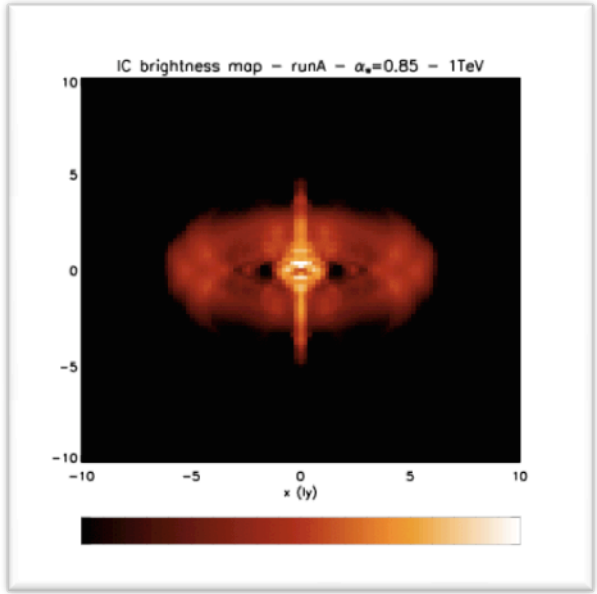

4 GeV 250 GeV 1 TeV

- Jet-torus structure should be visible in γ-rays
- Shrinkage of PWN size with increasing frequency

The Crab Nebula spectrum

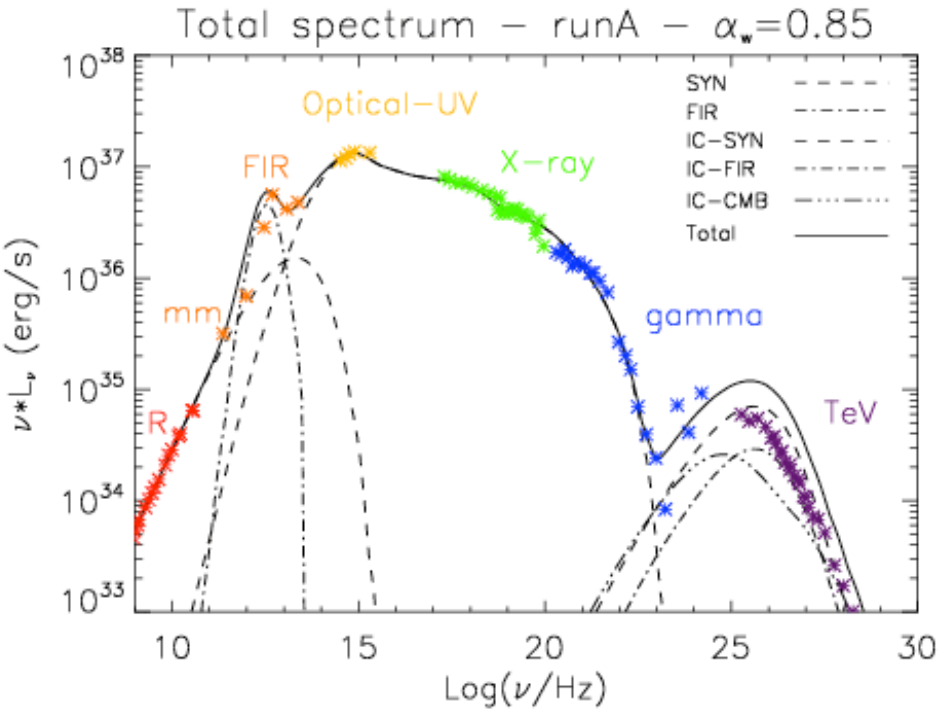

- Synchrotron spectrum fitted with α=0.85 (index -2.7)
- GeV emission agrees with Fermi-LAT (*Abdo et al., 2009*)
- TeV emission too high, average magnetic field too low?

Time variability: MHD origin

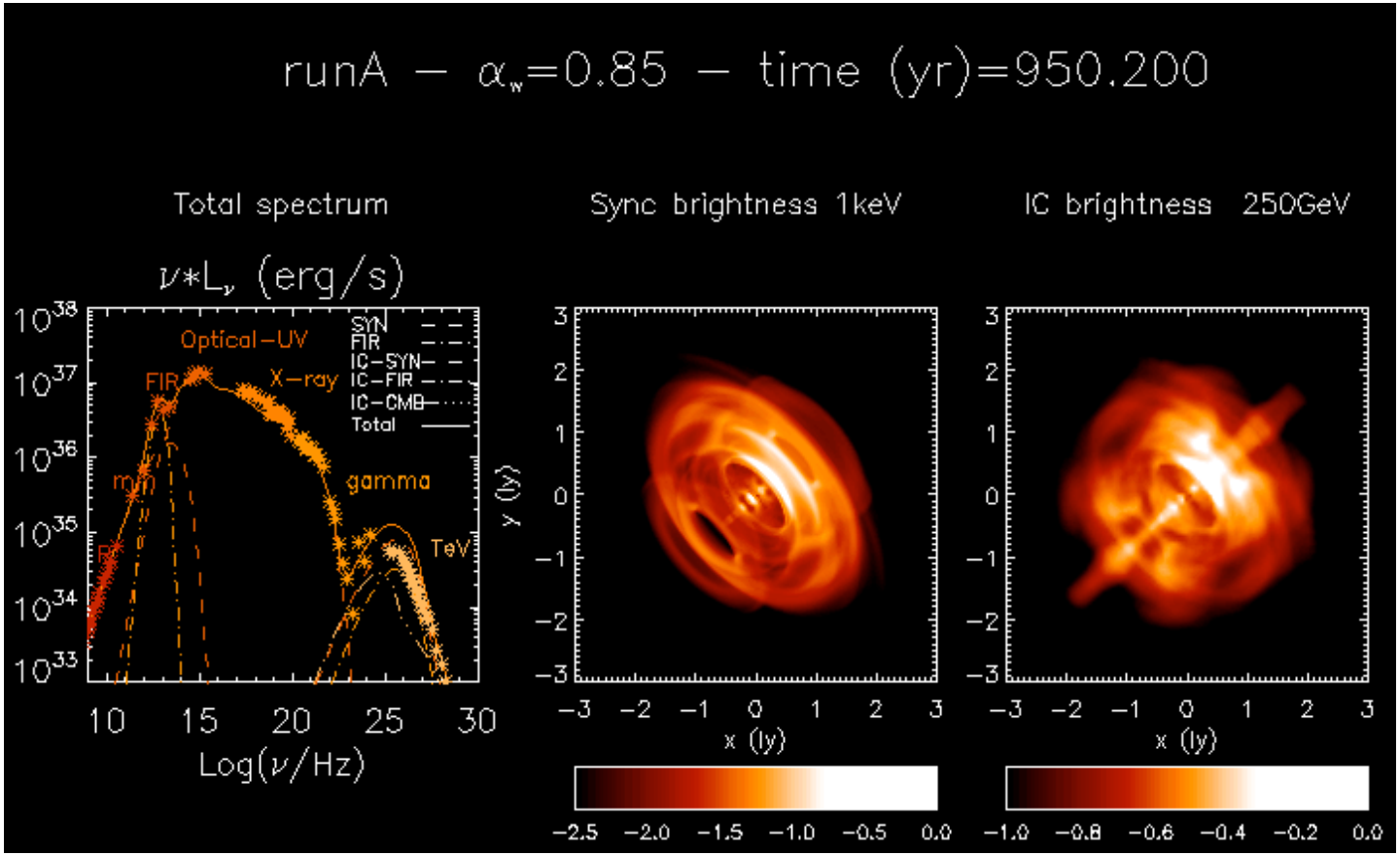

(Volpi et al., 2008)

Time variability - MHD origin

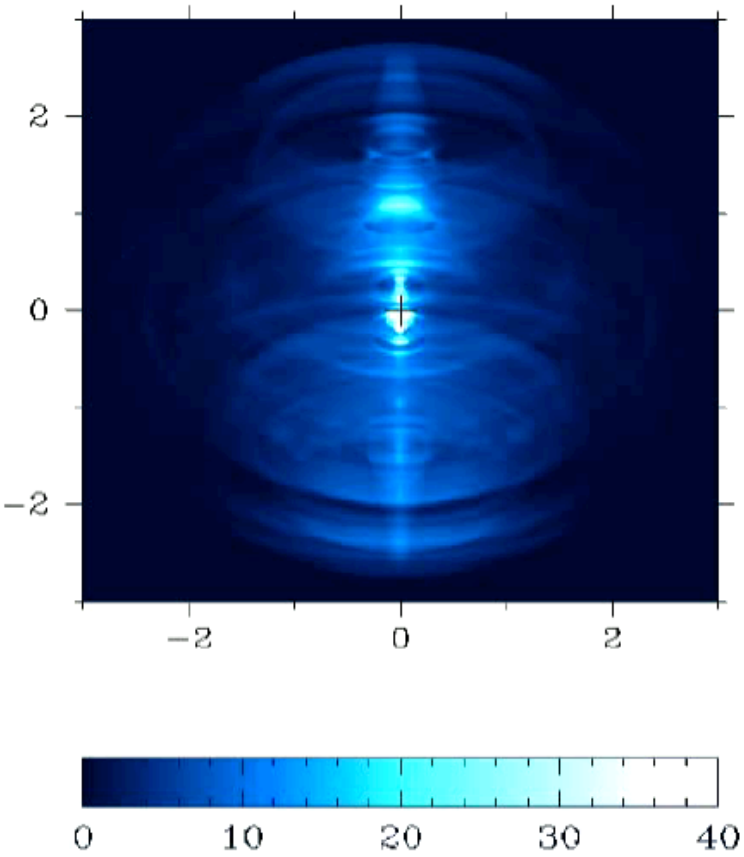

(Camus et al., 2009)

Outgoing wave pattern

Large luminosity variations

Features slow down as they move outward

Variability observed both in the knot and in the sprite

Pressure waves produce variability in the axial emissivity

observed timescales are recovered

Part II: LGRB jets from magnetars

- Long-duration GRBs are associated with core-collapse SNe, collimated relativistic jets must escape from the more massive and energetic ejecta (*Woosley & Bloom, 2006*)
- What is the central engine? We need 10^{52} erg in 10 sec!
- Mainstream model: collapsar (Kerr BH + disk)
  - Jets powered by neutrino heating (*MacFadyen, 1999; Aloy, 2000*)
  - Jets powered by BZ mechanism (*Barkov & Komissarov, 2008*)
- Alternative model: ms proto-magnetar with B~10^{15} G
  - Jets collimated by toroidal fields in a *Magnetar Wind Nebula*? (*Koenigl & Granot 2002; Bucciantini@UCBerkeley 2006-2009*)
  - Neutron stars are a natural outcome of core-collapse SNe, though fully self-consistent simulations are still missing

PNS wind regimes

Period increases and Luminosity drops

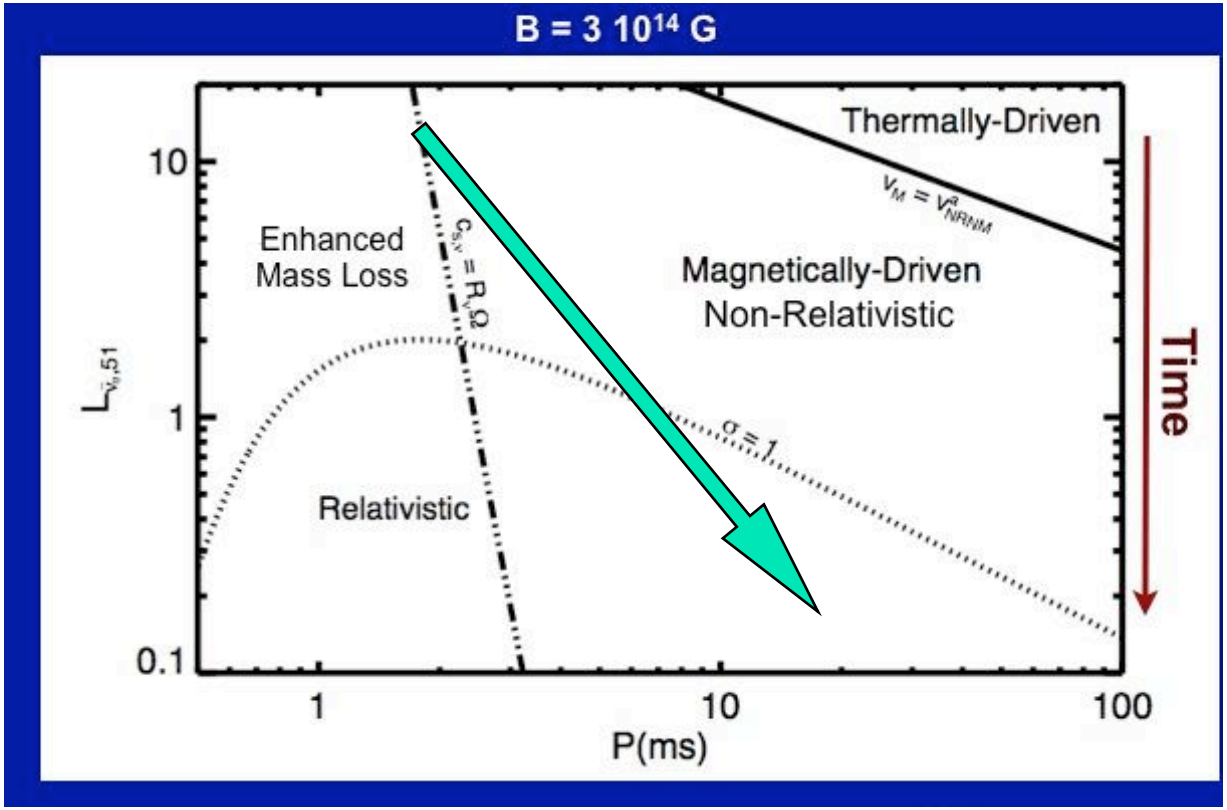

Metzger et al. 2007

Torque on the PNS

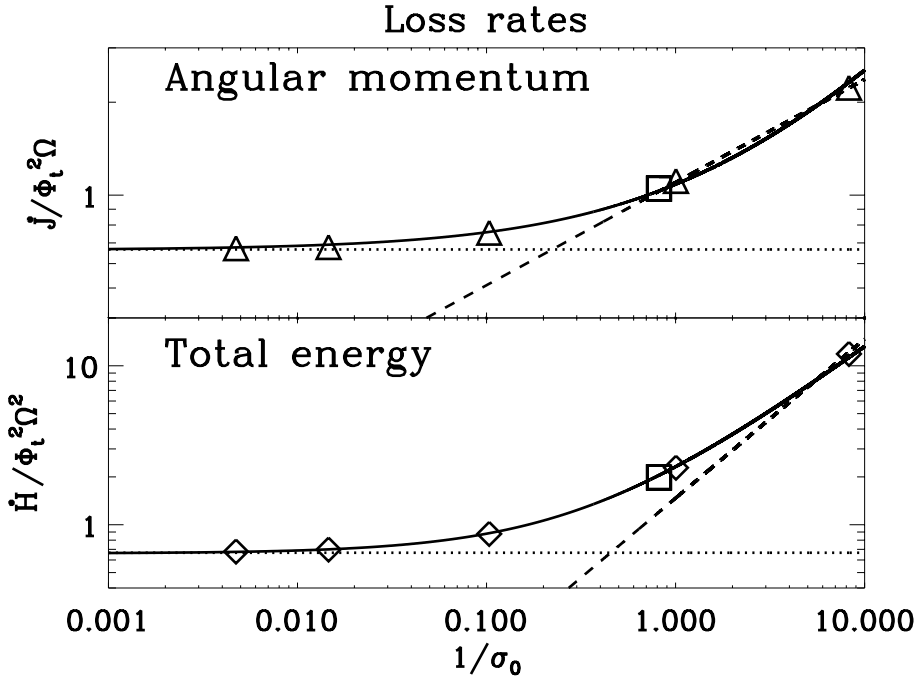

At early time σ < 1 angular momentum and energy losses are enhanced

At later time σ > 1 the losses converge to the FF value

Losses depend only on σ

Rapid cooling tend to favor GRB conditions - high available energy and high σ

Losses not affected by confinement inside progenitor

Magnetar outflows and GRBs

High energy jet

Early wind is favored in terms of dynamic properties

High Lorentz factor

Late force-free wind is favored for acceleration

The simultaneous requirement of collimation and acceleration excludes that LGRB are direct outflows from magnetars

What is the role of the confining progenitor?

The magnetar scenario

The magnetar scenario

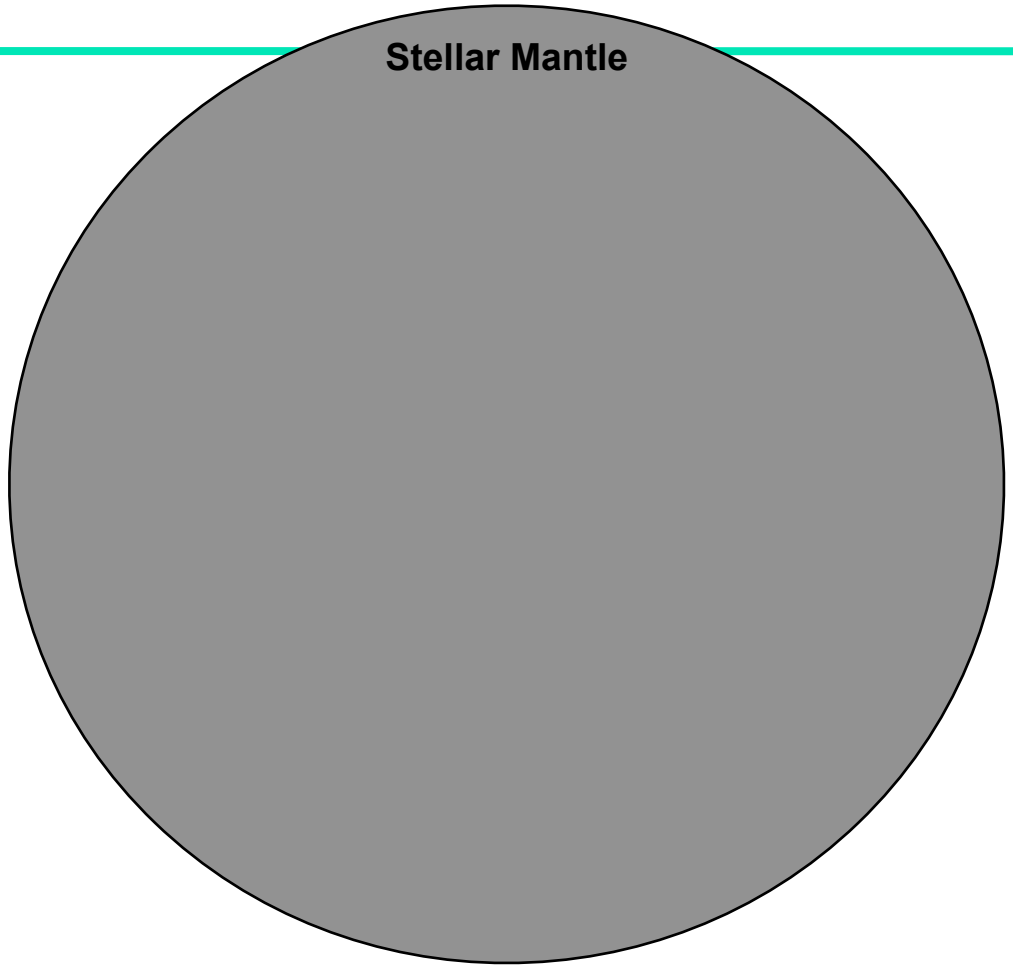

The magnetar scenario

Outgoing SN shock
V_{sn} ~ 0.03-0.05c
SN Shell creates a cavity

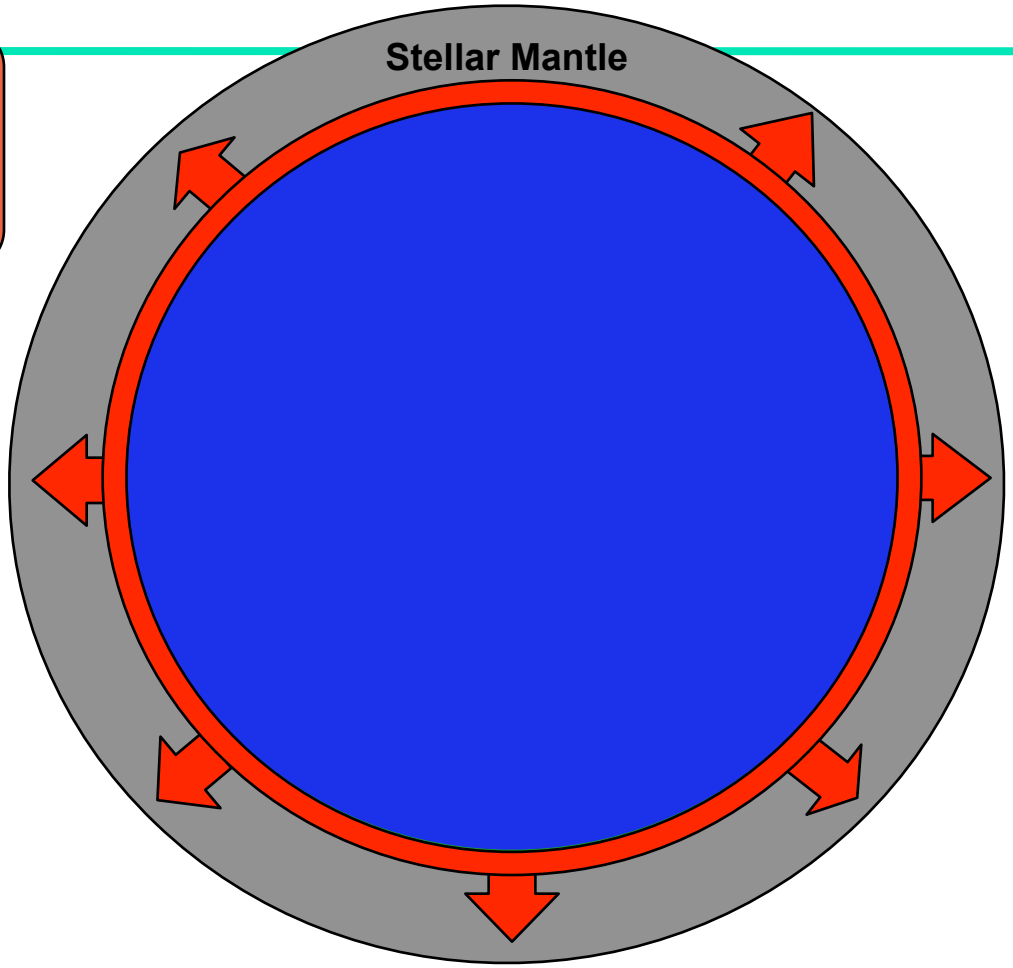

The magnetar scenario

Outgoing SN shock
V_{sn} ~ 0.03-0.05c
SN Shell creates a cavity

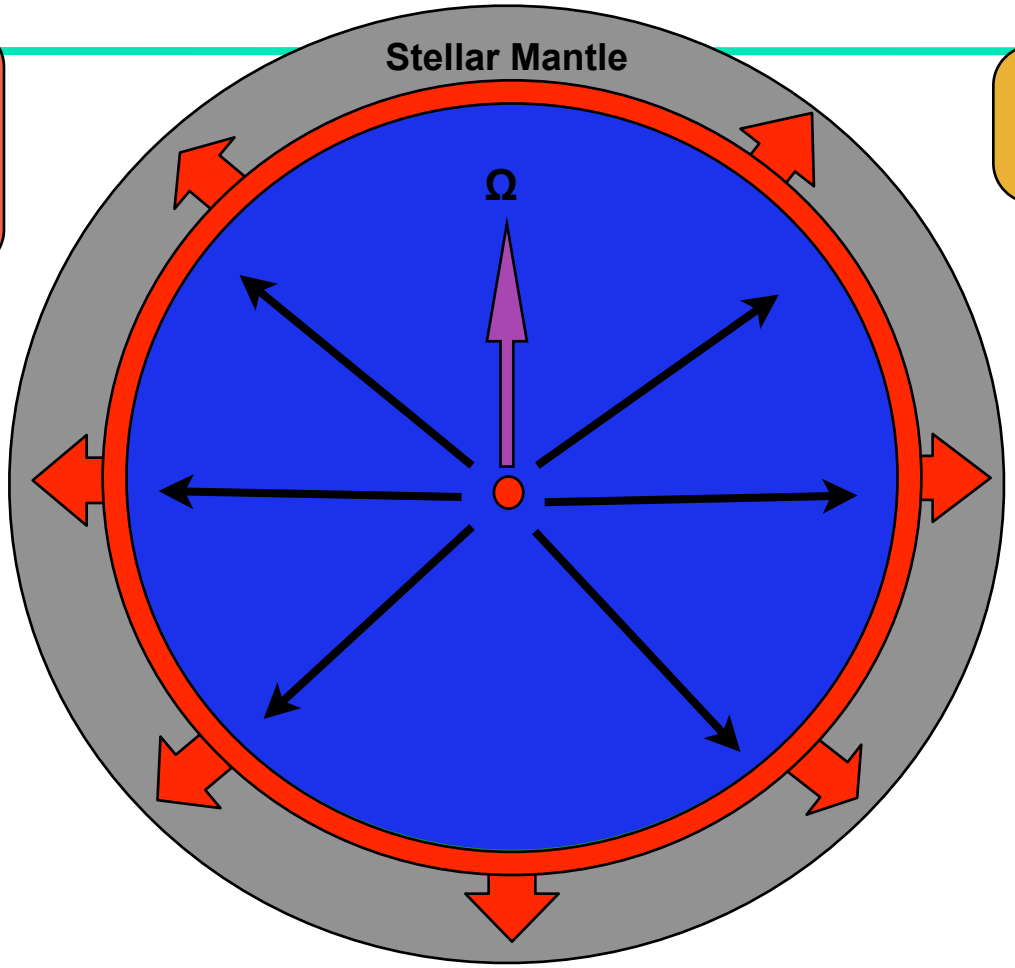

The cavity is swept by the PNS wind

The magnetar scenario

Outgoing SN shock
V_{sn} ~ 0.03-0.05c
SN Shell creates a cavity

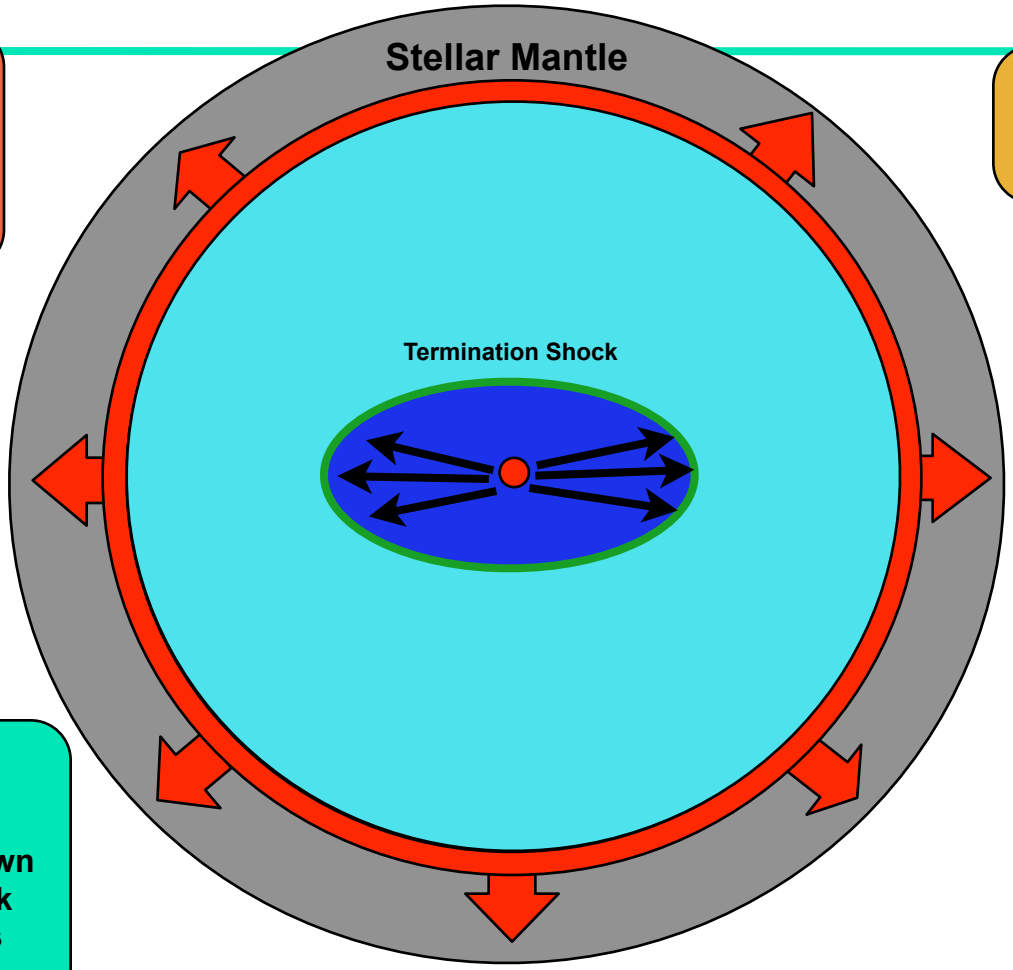

The cavity is swept by the PNS wind

$V_{sn} << V_{wind}$

The wind is slowed down in a termination shock
A Magnetar nebula is formed

The magnetar scenario

Outgoing SN shock
V_{sn} ~ 0.03-0.05c
SN Shell creates a cavity

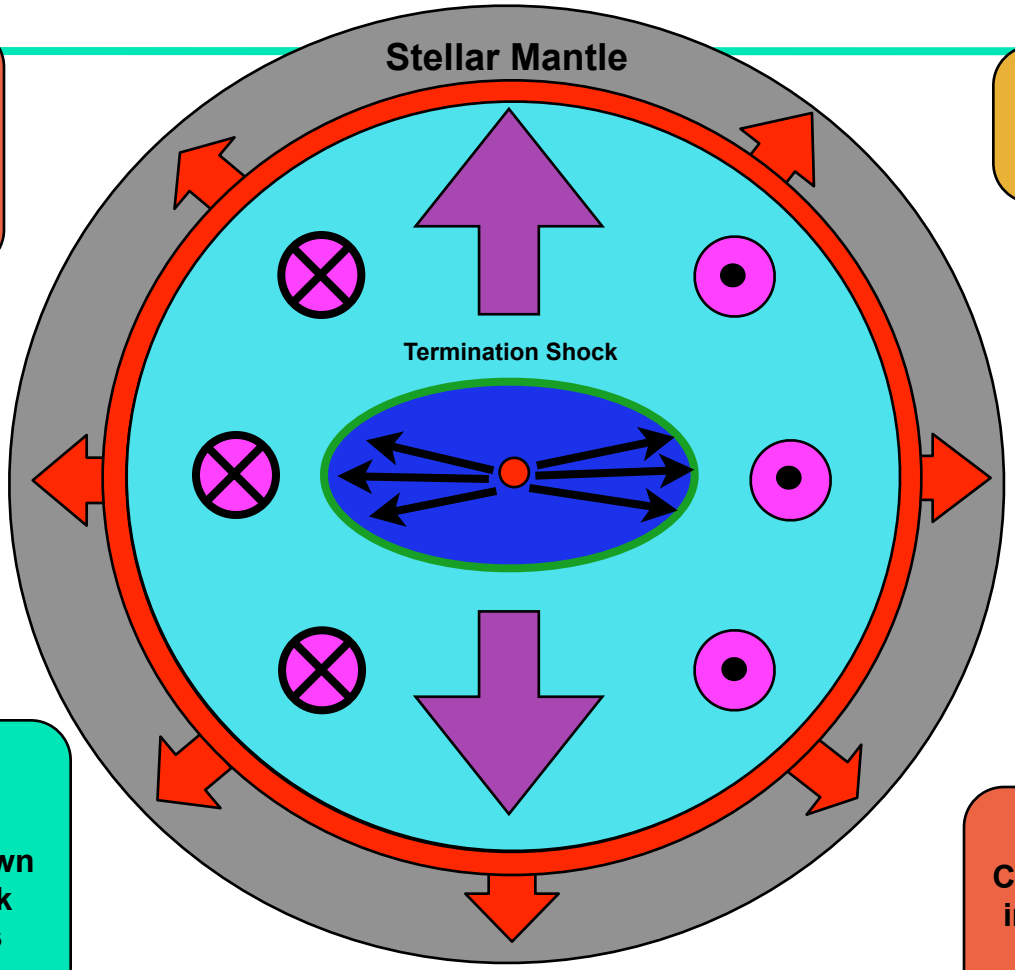

The cavity is swept by the PNS wind

$V_{sn} << V_{wind}$

The wind is slowed down in a termination shock
A Magnetar nebula is formed

Compressed magnetic field increases pressure on the axis

Toroidal fields and elongation in PWNe

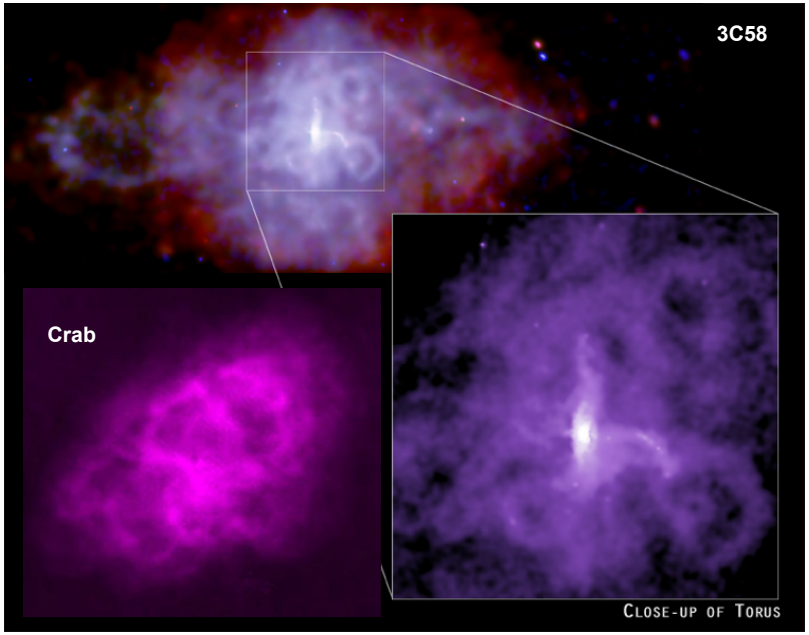

Confined toroidal magnetic field

Elongation along the rotation axis of the PSR

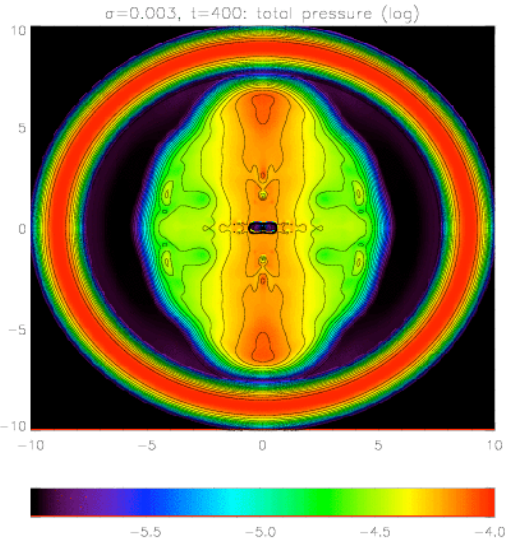

Del Zanna et al. 2004

The nebula elongation is independent of energy injection

Nebular pressure distribution

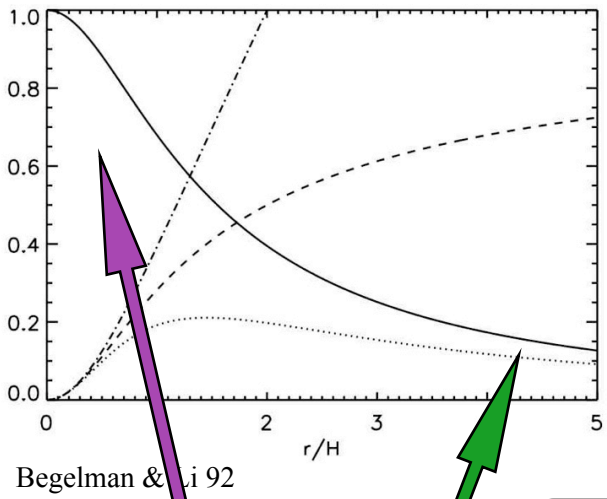

Begelman & Li 92

$V_{neb} << V_{wind} \sim c$

The evolution of the bubble is governed by the internal pressure distribution.

Compressed toroidal field creates *toothpaste effect*

Magnetic tension causes a redirection of momentum

Internal plasma pressure is higher on the axis than on the equator

→ Jet?

From elongated nebulae to jets?

What governs the transition from elongated structures to jets?

Magnetization in the nebula ➔ Wind magnetization

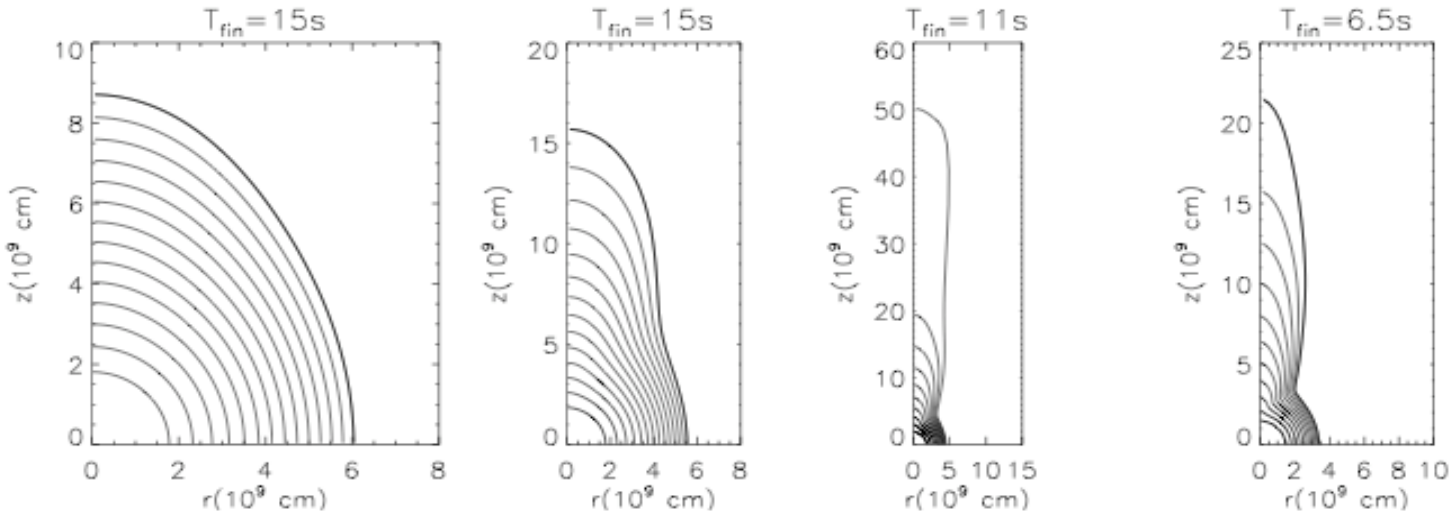

Bucciantini et al. 2007

PWN-like simulations

- Axisymmetric RMHD simulations with assigned wind conditions for the dissipative case as for PWNe (*Bucciantini et al. 2008*):

$$\dot{E} = 10^{51}\ erg/s, \quad \Gamma_w = 10, \quad \sigma = 0.1$$

- Full GRMHD (Schwarzschild metric) of wind launching from a ms rotating proto-magnetar and long-term jet evolution are now available (*Komissarov & Barkov 2008; Bucciantini, Quataert, Metzger, Thompson, Arons, Del Zanna, 2009*)

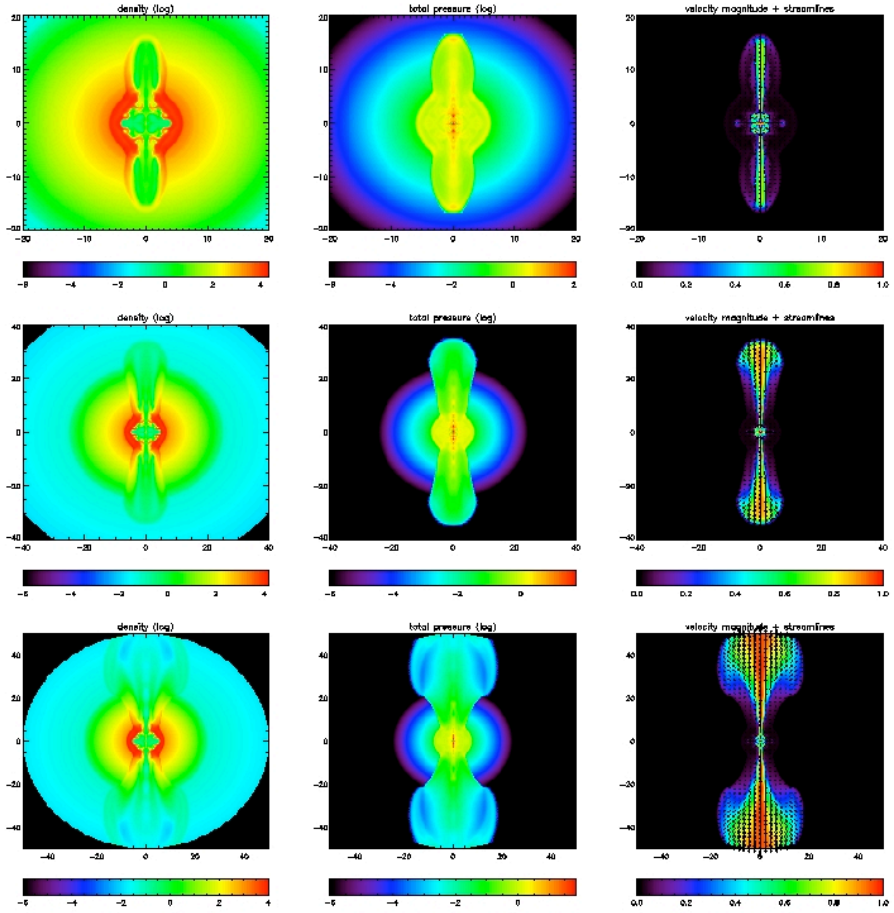

Figure 1. Evolution of a magnetized bubble inflated by a magnetar wind with $\dot{E} = 10^{51}$ erg s^{-1}, $\gamma_w = 10$ and $\sigma = 0.1$, inside a 35-$M_\odot$ progenitor star. From left to right: density (g cm^{-3}), pressure (g cm^{-3} c^2) and velocity (in units of c). From top to bottom: snapshots at 4, 5 and 6 s after core bounce. Distances are in 10^9 cm; the radius of the progenitor star is 2.5×10^{10} cm. By $t = 5$ s (middle panel) the jet has escaped the progenitor star.

Wind launching and jet collimation

Recent numerical study investigates the transition from the matter dominated phase to the magnetic dominated phase

Wind launching and jet collimation

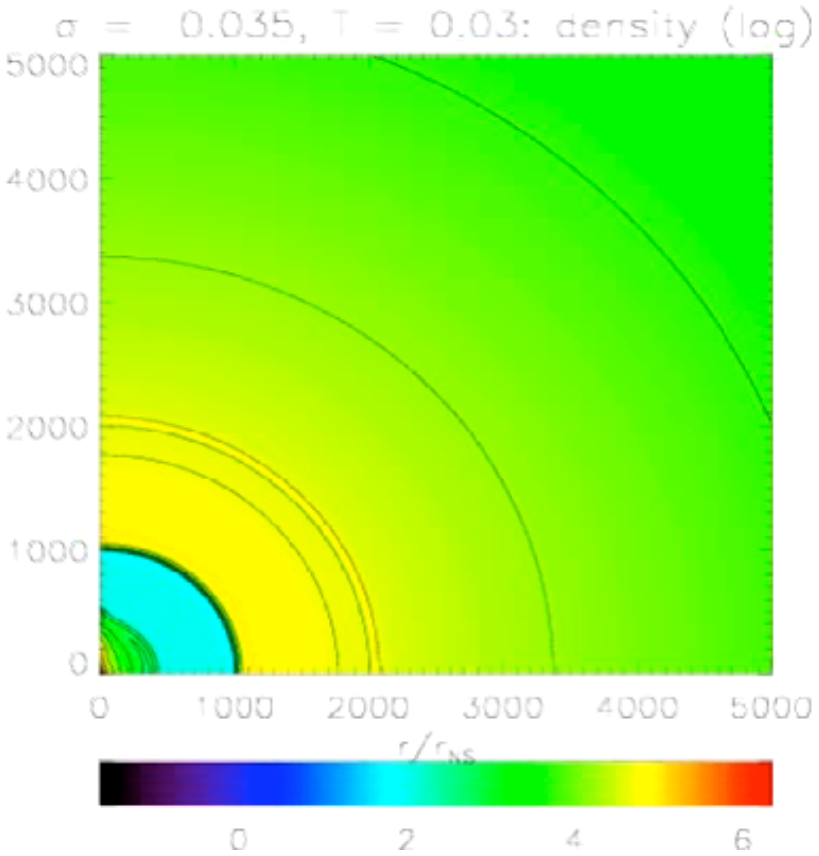

Recent numerical study investigates the transition from the matter dominated phase to the magnetic dominated phase

Wind launching and jet collimation

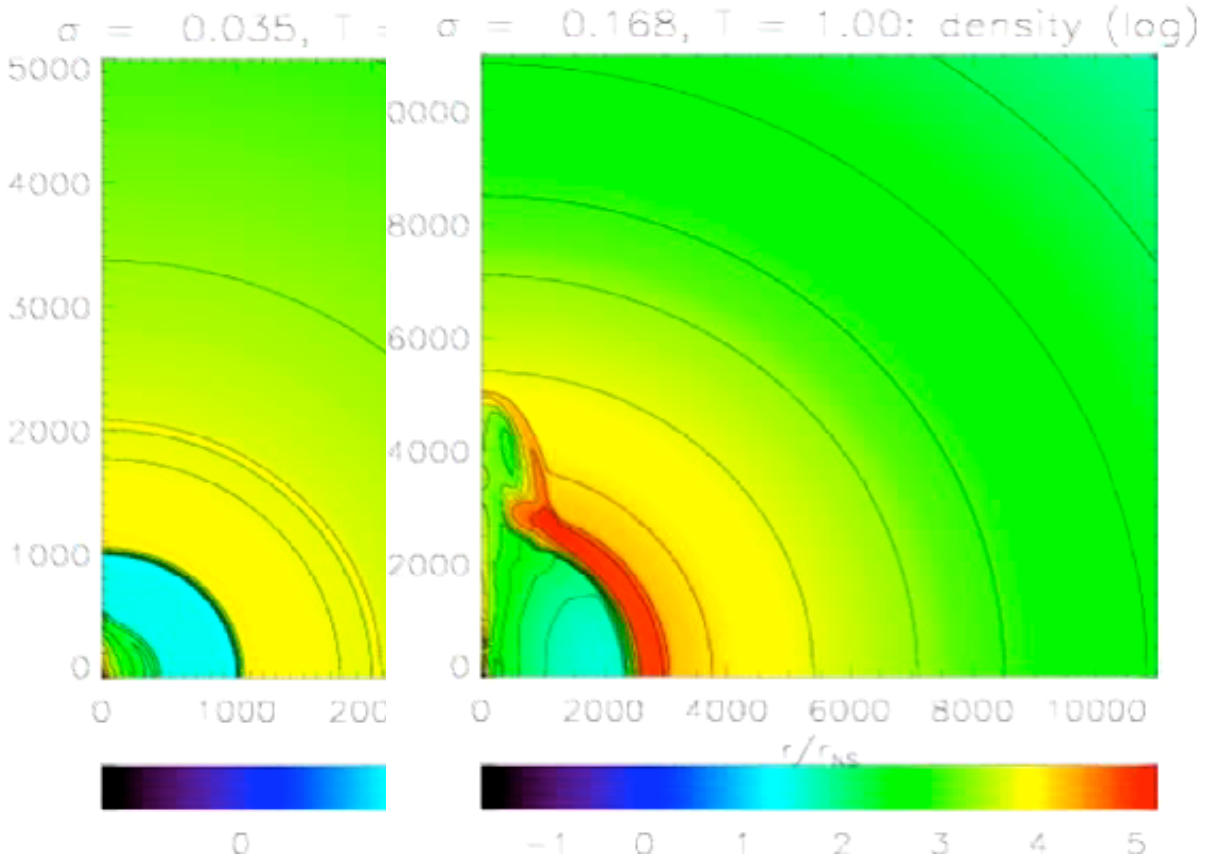

**umerical study
stigates the
from the matter
ed phase to the
tic dominated
phase**

Wind launching and jet collimation

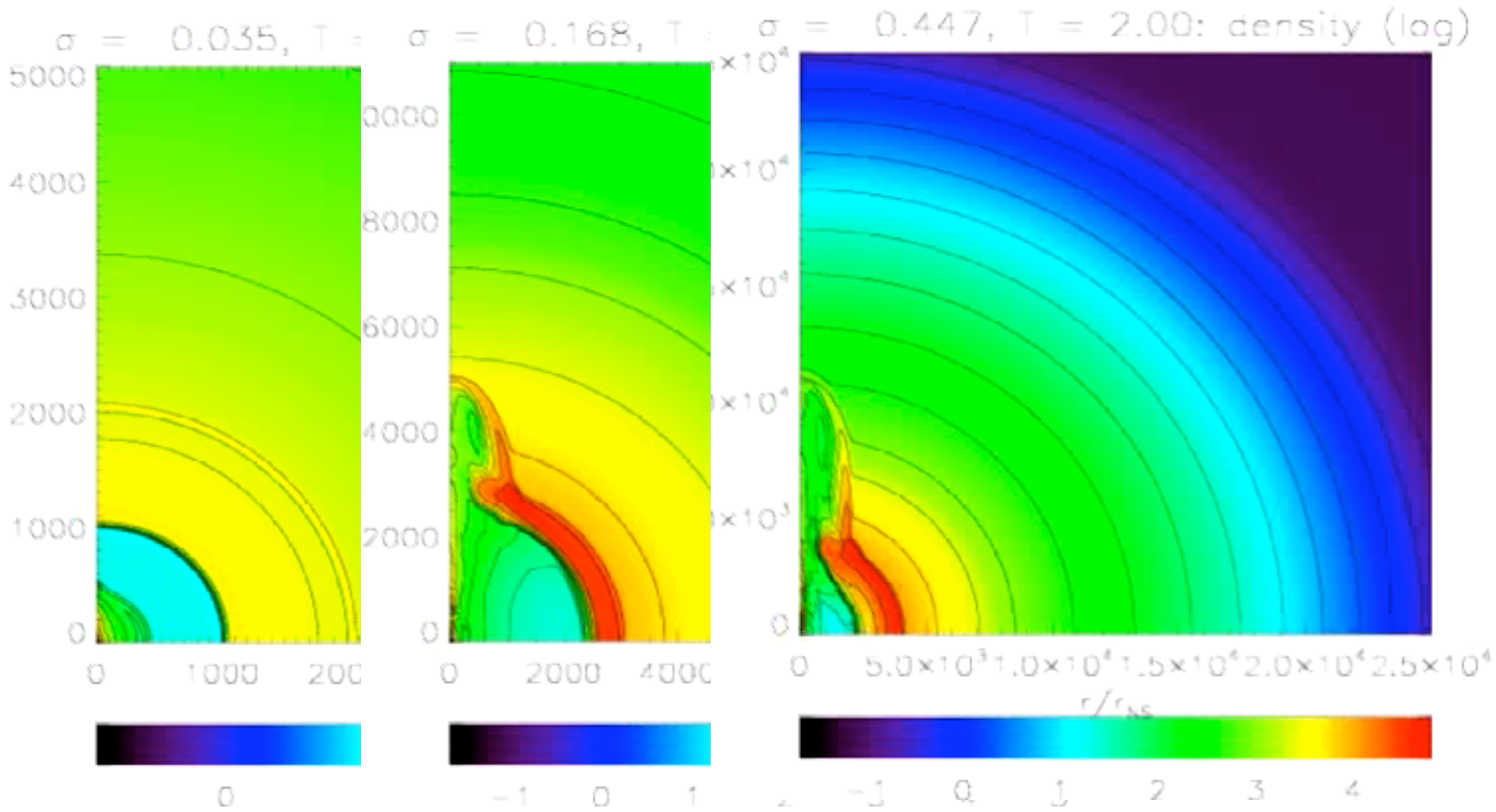

Late time evolution: the jet escapes

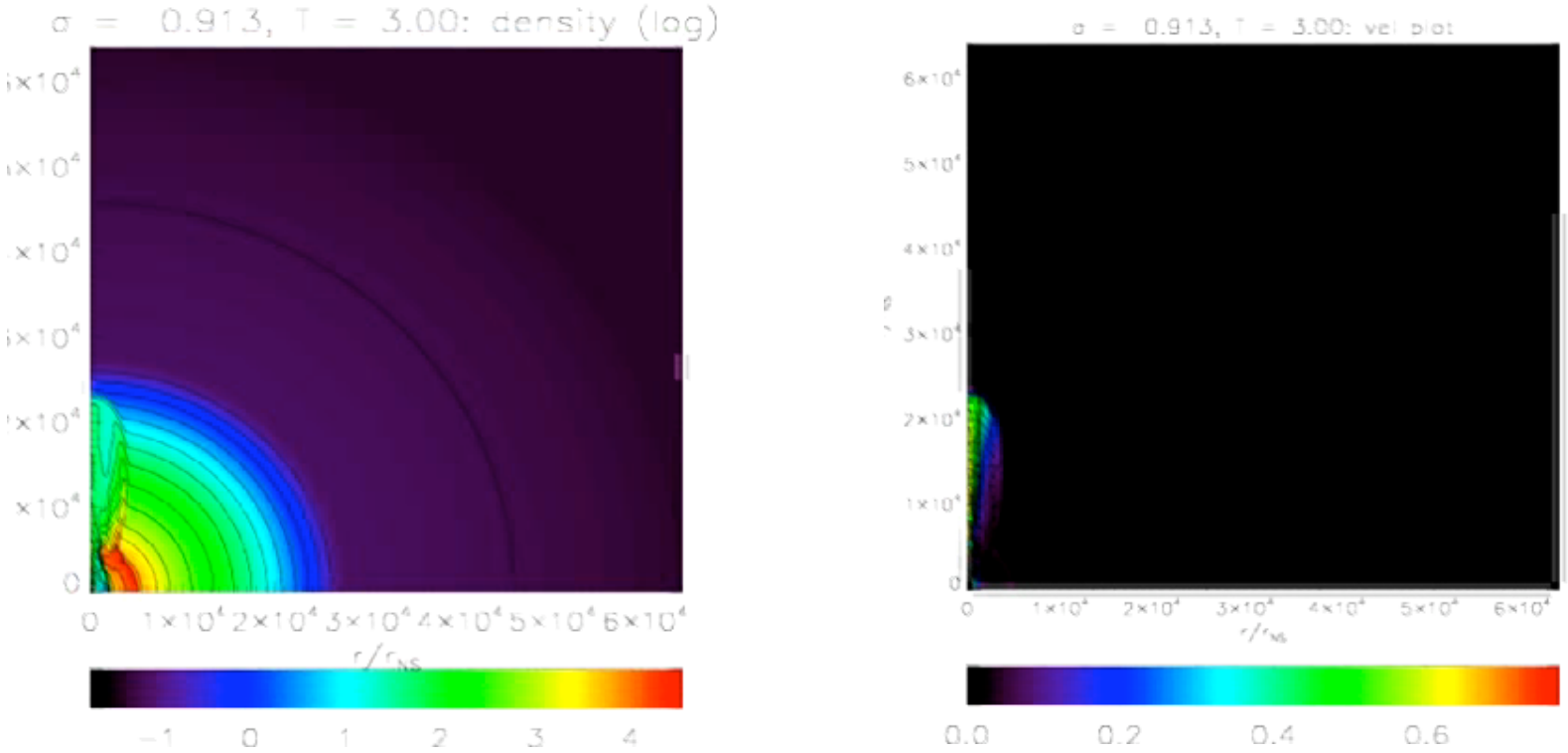

dt ~ 3 10^{-7} sec - T_{fin} ~ 10 sec

3 10^{7} steps - (necessary to resolve the NS heating zone)

dr = 2 10^{4} cm - R = 6 10^{10} cm

Part III: the ECHO code and beyond...

- Eulerian Conservative High Order code: the aim is to combine shock-capturing properties and accuracy for small scale wave propagation and turbulence, in a 3+1 approach
  - *L. Del Zanna, O. Zanotti, N. Bucciantini, P. Londrillo, 2007, A&A 473, 11*
  - GR upgrade of: *Del Zanna & Bucciantini 2002*; *Del Zanna et al. 2003*
- Modular structure, F90 language, MPI parallelization
- Many physical modules (MHD, RMHD, GRMHD, GRMD,…)
- Any metric allowed (1-,2- or 3-D), even time-dependent
- Finite-difference scheme, Runge-Kutta time-stepping
- UCT strategy for the magnetic field (*Londrillo & Del Zanna 2000, 2004*)
- High-order reconstruction procedures (explicit and implicit)
- Central-type Riemann solvers (our most succesfull recipe!)

ECHO: Eulerian 3+1 approach for GRMHD

- Set of 8 conservation laws + 1 constraint:

$$\partial_t(\sqrt{\gamma}\,D) + \partial_i[\sqrt{\gamma}\,(\alpha v^i - \beta^i)D] = 0$$

$$\partial_t(\sqrt{\gamma}\,S_j) + \partial_i[\sqrt{\gamma}\,(\alpha W^i_j - \beta^i S_j)] = \sqrt{\gamma}\,(\alpha W^{ik}\partial_j \gamma_{ik}/2 + S_i\partial_j\beta^i - U\partial_j\alpha)$$

$$\partial_t(\sqrt{\gamma}\,U) + \partial_i[\sqrt{\gamma}\,(\alpha S^i - \beta^i U)] = \sqrt{\gamma}\,(\alpha K_{ij}W^{ij} - S^i\partial_i\alpha)$$

$$\partial_t(\sqrt{\gamma}\,B^j) + \partial_i[\sqrt{\gamma}\,(\alpha v^i - \beta^i)B^j - \sqrt{\gamma}\,(\alpha v^j - \beta^j)B^i] = 0; \quad \partial_i(\sqrt{\gamma}\,B^i) = 0$$

- No Lie derivatives nor Christoffel symbols needed in source terms
- The lapse function α, shift vector β, metric tensor γ and the extrinsic curvature **K** may be time-dependent (evolved through Einstein's eqs.)
- Only familiar <u>spatial 3-D</u> vectors and tensors, easy RMHD and MHD limits

$$D = \rho\Gamma; \quad \vec{S} = \rho h\Gamma^2\vec{v} + \vec{E}\times\vec{B}; \quad U = \rho h\Gamma^2 - p + (E^2 + B^2)/2$$

$$\vec{\vec{W}} = \rho h\Gamma^2\vec{v}\vec{v} + p\vec{\vec{\gamma}} - \vec{E}\vec{E} - \vec{B}\vec{B} + (E^2 + B^2)/2\vec{\vec{\gamma}}; \quad \vec{E} = -\vec{v}\times\vec{B}$$

ECHO: FD-UCT discretization strategy

- The two sets of conservation laws are discretized in space according the Upwind Constrained Transport strategies (UCT: *Londrillo & Del Zanna ApJ 530, 508, 2000; JCP 195, 17, 2004*)
  - Staggered grid for magnetic and electric field components
  - Finite differences: point values at cell centers (u), at cell faces (b and f), at edges (e). The *hat* indicates high-order differencing

$$\frac{d}{dt}[u_j]_C + \sum_i \frac{1}{h_i}([\hat{f}^i_j]_{S_i^+} - [\hat{f}^i_j]_{S_i^-}) = [s_j]_C$$

$$\frac{d}{dt}[b^i]_{S_i^+} + \sum_{j,k}[ijk]\frac{1}{h_j}([\hat{e}_k]_{L_k^+} - [\hat{e}_k]_{L_k^-}) = 0; \quad \sum_i \frac{1}{h_i}([\hat{b}^i]_{S_i^+} - [\hat{b}^i]_{S_i^-}) = 0$$

- The solenoidal constraint is maintained <u>algebraically</u> regardless of the order of the scheme

Numerical tests: convergence

- A large-amplitude CP Alfvén wave is an exact solution for both MHD and RMHD (here E is important, Va is modified)
- Convergence is measured on any quantity u after one period T of propagation along the diagonal of a 2-D periodical box:

$$L_1(u) = \sum_{ij} |u(x_i, y_j, T) - u(x_i, y_j, 0)| / N^2 \propto N^{-r}$$

$$B_y = \eta B_0 \cos(x - v_A t), \quad v_y = -v_A B_y / B_0$$
$$B_z = \eta B_0 \sin(x - v_A t), \quad v_z = -v_A B_z / B_0$$

$$v_A^2 = \frac{B_0^2}{\rho h + (1+\eta^2) B_0^2} \left\{ \frac{1 + \sqrt{1 - 4\eta^2 B_0^2 / [\rho h + (1+\eta^2) B_0^2]}}{2} \right\}^{-1}$$

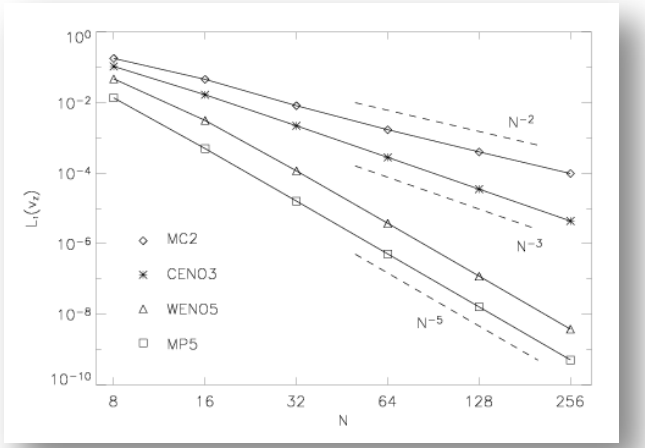

Numerical tests: thick disk in Kerr metric

- Results for t=200, approximately 3 rotation periods, with MP5, RK2

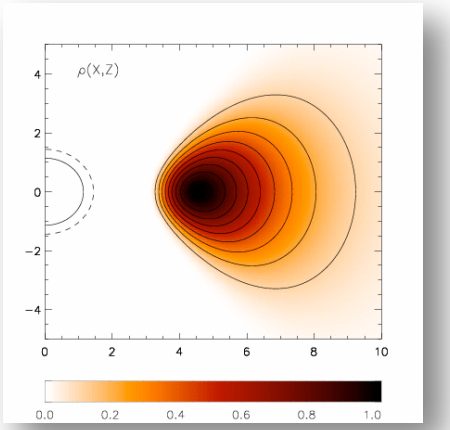

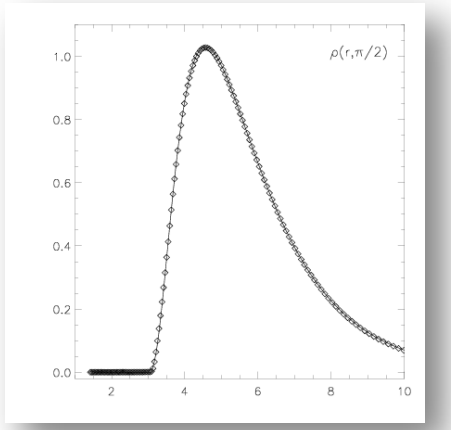

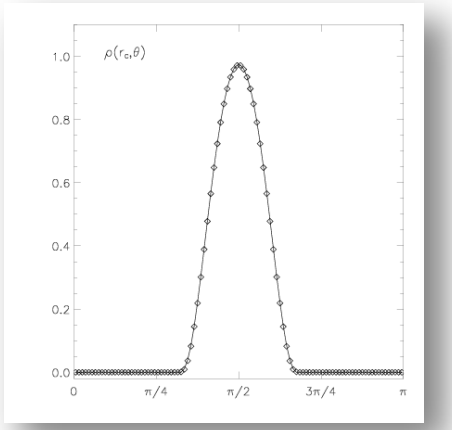

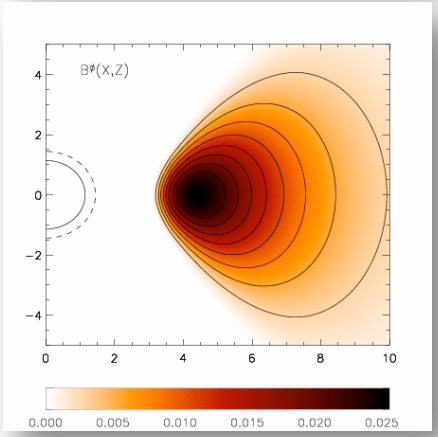

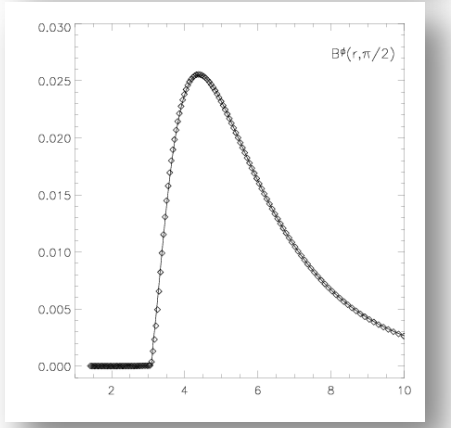

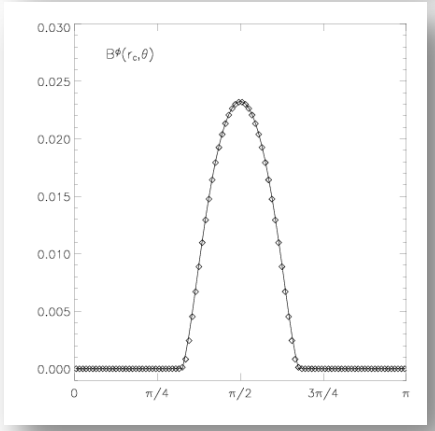

Circumbinary disks of SMBHs

- The circumbinary disk in the post-merger phase of SMBHs is affected by mass loss and recoil of the resulting SMBH
- 2-D GRMHD simulations of kicked disks are being performed with ECHO (*Zanotti, Rezzolla, Del Zanna, Palenzuela, in prep.*)

Circumbinary disks of SMBHs

- The circumbinary disk in the post-merger phase of SMBHs is affected by mass loss and recoil of the resulting SMBH
- 2-D GRMHD simulations of kicked disks are being performed with ECHO (*Zanotti, Rezzolla, Del Zanna, Palenzuela, in prep.*)

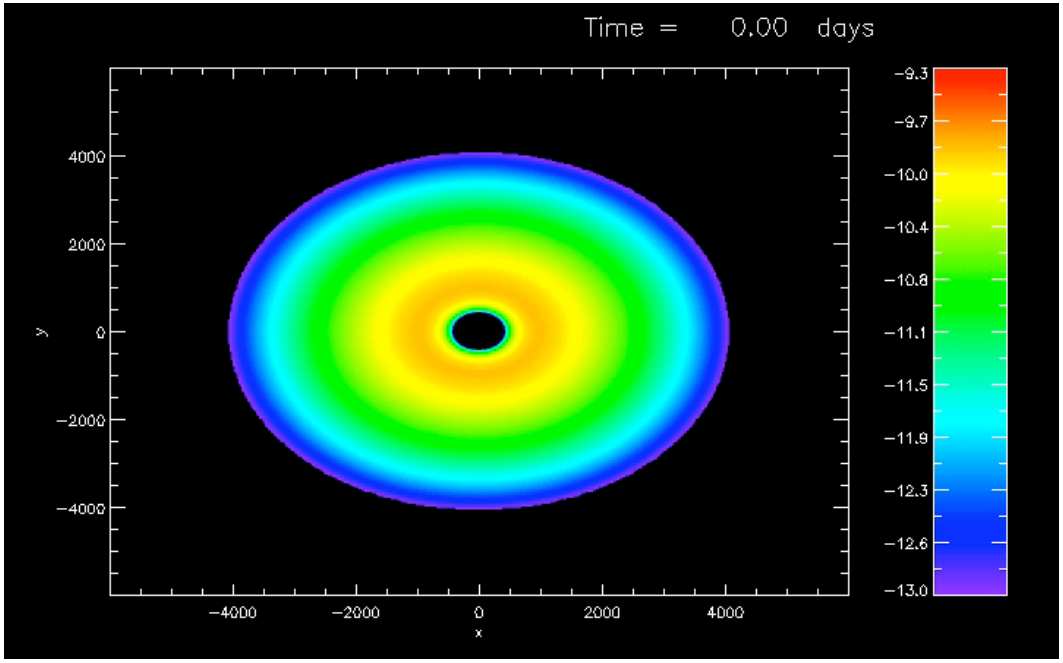

Towards collapse to proto-magnetars...

- ECHO has been recently coupled to an Einstein solver in axisymmetry: XCFC elliptic equations with both conformal flatness and local uniqness guaranteed (*Cordero-Carrion et al., 2009*)
- We use a mixed spectral/implicit method (spherical harmonics + finite differences and matrix inversion)

$$\Delta X^i + \tfrac{1}{3}\mathcal{D}^i\mathcal{D}_j X^j = 8\pi f^{ij} S^*_j,$$

$$\hat{A}^{ij} = (LX)^{ij} = \mathcal{D}^i X^j + \mathcal{D}^j X^i - \tfrac{2}{3}\mathcal{D}_k X^k f^{ij}.$$

$$\Delta\psi = -2\pi\psi^{-1}E^* - \psi^{-7}\frac{f_{il}f_{jm}\hat{A}^{lm}\hat{A}^{ij}}{8}.$$

$$\Delta(\psi N) = 2\pi N\psi^{-1}(E^* + 2S^*) + N\psi^{-7}\frac{7f_{il}f_{jm}\hat{A}^{lm}\hat{A}^{ij}}{8}.$$

$$\Delta\beta^i + \tfrac{1}{3}\mathcal{D}^i(\mathcal{D}_j\beta^j) = \mathcal{D}_j(2N\psi^{-6}\hat{A}^{ij}),$$

Towards collapse to proto-magnetars...

- First test: normal modes of oscillations of a polytropic NS in isotropic coordinates are recovered (*Bucciantini et al., yesterday!*)
- Comparison of *exact* and XCFC-ECHO power spectrum

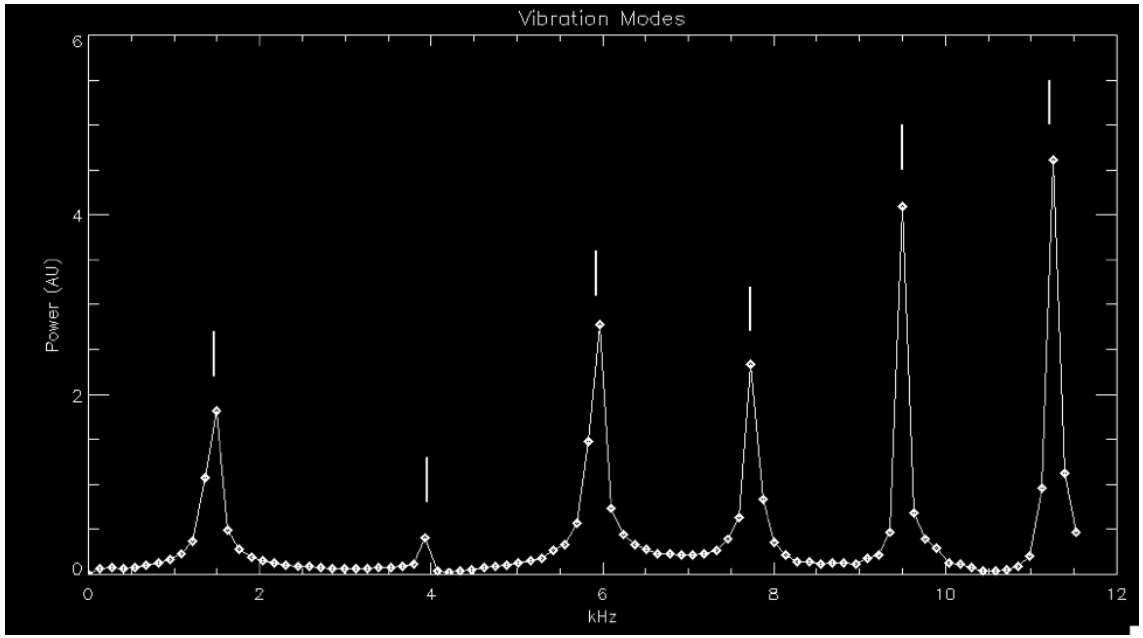

Conclusions

- Relativistic jets in PWNe and in LGRB progenitors may share a common mechanism of magnetic collimation:
- Pulsar Wind Nebulae
  - Jet-torus structure, jet collimation explained by hoop stresses
  - Complete set of synchrotron and IC diagnostic tools
  - Finest details reproduced: flows and vortices around TS
  - Time variability reproduced: MHD origin
- LGRBs powered by proto-magnetar winds
  - Jet collimation due to hoop stresses in a magnetar wind nebula
  - First long-term simulations from wind launching to jet escape
  - Future: towards more realistic post core-collapse PNS conditions?

Conclusions

- Relativistic jets in PWNe and in LGRB progenitors may share a common mechanism of magnetic collimation:
- Pulsar Wind Nebulae
  - Jet-torus structure, jet collimation explained by hoop stresses
  - Complete set of synchrotron and IC diagnostic tools
  - Finest details reproduced: flows and vortices around TS
  - Time variability reproduced: MHD origin
- LGRBs powered by proto-magnetar winds
  - Jet collimation due to hoop stresses in a magnetar wind nebula
  - First long-term simulations from wind launching to jet escape
  - Future: towards more realistic post core-collapse PNS conditions?

Thank you!